AGU PUBLICATIONS

JGR

Journal of Geophysical Research: Oceans

RESEARCH ARTICLE

10.1002/2016JC011818

Special Section:
Dense water formations in the North Western Mediterranean: from the physical forcings to the biogeochemical consequences

Budget of organic carbon in the North-Western Mediterranean open sea over the period 2004–2008 using 3-D coupled physical-biogeochemical modeling

C. Ulses[1], P.-A. Auger[1,2], K. Soetaert[3], P. Marsaleix[1], F. Diaz[4], L. Coppola[5], M.J. Herrmann[6], F. Kessouri[1,7], and C. Estournel[1]

[1]Laboratoire d'Aérologie, Université de Toulouse, CNRS, UPS, Toulouse, France, [2]Instituto Milenio de Oceanografía and Escuela de Ciencias del Mar, Pontificia Universidad Católica de Valparaíso, Valparaíso, Chile, [3]Department of Estuarine and Delta Systems, NIOZ Royal Netherlands Institute for Sea Research, and Utrecht University, Yerseke, Netherlands, [4]Aix Marseille Univ, Univ Toulon, CNRS, IRD, Mediterranean Institute of Oceanography UM110, Marseille, France, [5]Sorbonne Universités, UPMC Université Paris 06, CNRS, Laboratoire d'océanographie de Villefranche, Observatoire Océanologique, Villefranche-sur-Mer, France, [6]Laboratoire d'Etudes en Géophysique et Océanographie Spatiales, UMR 5566, CNRS-CNES-IRD-Université de Toulouse, Toulouse, France, [7]Department of Atmospheric and Oceanic Sciences, University of California, Los Angeles, Los Angeles, California, USA

Key Points:
- A budget of organic carbon is estimated using 3-D physical-biogeochemical coupled modeling
- The interannual variability of primary production and downward export is assessed

Correspondence to:
C. Ulses,
caroline.ulses@aero.obs-mip.fr

Citation:
Ulses, C., P.-A. Auger, K. Soetaert, P. Marsaleix, F. Diaz, L. Coppola, M.J. Herrmann, F. Kessouri, and C. Estournel (2016), Budget of organic carbon in the North-Western Mediterranean open sea over the period 2004–2008 using 3-D coupled physical-biogeochemical modeling, *J. Geophys. Res. Oceans*, *121*, 7026–7055, doi:10.1002/2016JC011818.

Received 21 MAR 2016
Accepted 12 AUG 2016
Accepted article online 18 AUG 2016
Published online 24 SEP 2016
Corrected 11 OCT 2016

This article was corrected on 11 OCT 2016. See the end of the full text for details.

Abstract A 3-D hydrodynamic-biogeochemical coupled model has been used to estimate a budget of organic carbon and its interannual variability over the 5 year period 2004–2008 in the North-Western Mediterranean Open Sea (NWMOS). The comparison of its results with in situ and satellite observations reveals that the timing and the magnitude of the convection and bloom processes during the study period, marked by contrasted atmospheric conditions, are reasonably well reproduced by the model. Model outputs show that the amount of nutrients annually injected into the surface layer is clearly linked to the intensity of the events of winter convection. During cold winters, primary production is reduced by intense mixing events but then spectacularly increases when the water column restratifies. In contrast, during mild winters, the primary production progressively and continuously increases, sustained by moderate new production followed by regenerated production. Overall, interannual variability in the annual primary production is low. The export in subsurface and at middepth is however affected by the intensity of the convection process, with annual values twice as high during cold winters than during mild winters. Finally, the estimation of a global budget of organic carbon reveals that the NWMOS acts as a sink for the shallower areas and as a source for the Algerian and Balearic subbasins.

1. Introduction

The Mediterranean Sea displays various hydrodynamic and ecological regimes, with a general west-east oligotroph gradient. Using satellite data, *D'Ortenzio and Ribera d'Alcala* [2009] evidenced blooming regimes, as in temperate regions, and nonblooming regimes, as in subtropical regions characterized by a low seasonal variation with a winter plateau rather than a clear peak in phytoplankton biomass. The North-Western Mediterranean Open Sea (NWMOS, Figure 1) is the region where the bloom is the most intense in the basin, owing to the strength of the deep convection process. During winter mixing episodes, large amounts of nutrients are injected from the deep ocean to the photic zone, where they sustain an explosive bloom in late winter/early spring. In parallel, this region is the place of the formation of the Western Mediterranean Deep Water (WMDW) which may disperse in the entire western subbasin [*Schroeder et al*., 2008]. Previous studies evidenced the large downward export of particulate and dissolved organic carbon (POC and DOC), accumulated during stratified periods in the euphotic layer, occurring during this open-ocean WMDW formation [*Migon et al*., 2002; *Santinelli et al*., 2010; *Stabholz et al*., 2013]. Therefore this latter process may drive modifications in biogeochemical compounds in the deep sea and consequently in deep biological activities and benthic habitats in the western subbasin.

The interannual variability of the open-sea convection with respect to timing, intensity, and spatial extent has been shown to be mostly linked to meteorological forcings [*Mertens and Schott*, 1998; *Béthoux et al*.,

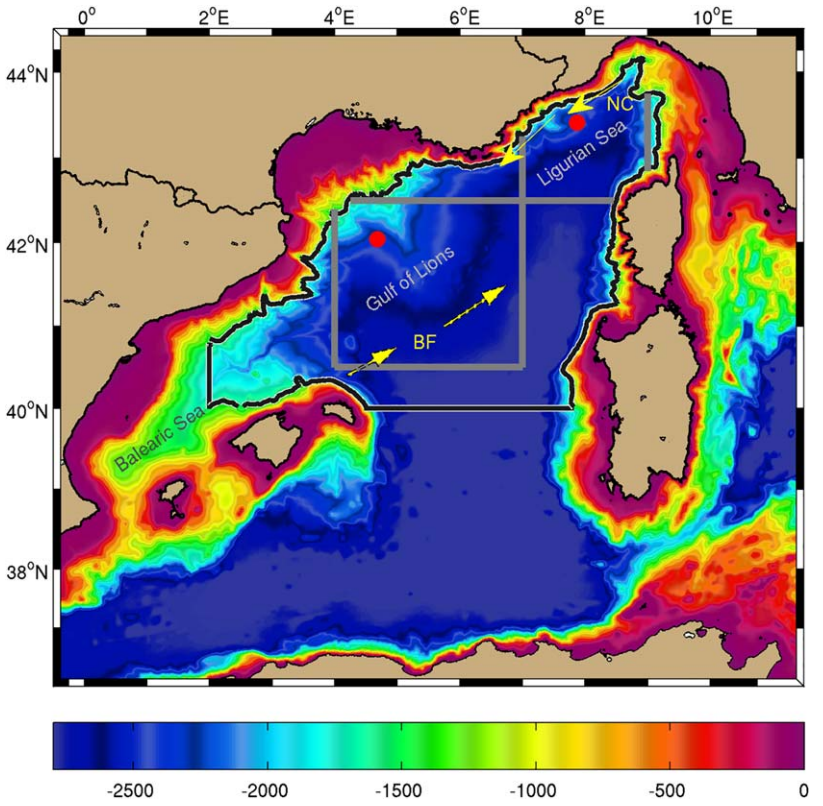

Figure 1. Model domain and bathymetry (m). The area of analysis, the North-Western Mediterranean Open Sea (NWMOS, 2°E < longitude < 9.5°N; 40°N < latitude< 45°N; bathymetry > 1500 m) is delimited by the thick black and white line. Grey boxes indicate the "MEDOC box" and the "Ligure box." NC indicates the Northern Current, and BF the Balearic front. Red points indicate "LION" site (42° 2.5′ N; 4° 41′ E) and DYFAMED site (43° 25′ N; 7° 52′ E).

2002; *Herrmann et al*., 2010; *Houpert*, 2013]. This variability may lead to an interannual variability of the amount of nutrients brought up into the surface layer, as well as of the amount of organic matter produced in the photic zone and of its downward transfer to the deep sea. Several observational studies investigated the interannual variability of the biogeochemical fluxes during the last decades. *Bosc et al*. [2004] estimated a low interannual variability in primary production in the NWMOS by analyzing 4 year SeaWiFS satellite surface chlorophyll concentrations, while *Marty and Chiavérini* [2002] inferred high fluctuations in annual production in the Ligurian Sea, based on 7 year monthly in situ measurements. *Lavigne et al*. [2013], based on analyses of satellite data, indicated that the annual ecosystem dynamics may oscillate between blooming and nonblooming regimes, depending on meteorological factors (i.e., wind stress and heat fluxes). They showed that the interannual variability of the intensity of the winter mixing appeared higher than the one of the maximum value of surface chlorophyll concentration. They hypothesized therefore that additional factors, besides the sole winter mixing may influence the biogeochemical activity in the productive layer. Moreover *Stabholz et al*. [2013] showed an increase in not only the downward total matter fluxes but also the associated POC fluxes in the NWMOS, during a vigorous winter compared to a mild convection winter. However these observational studies relied on surface-restricted satellite data or on in situ measurements exploring the water column but limited in space and time. Three-dimensional hydrodynamic-biogeochemical coupled models are useful tools to overcome these issues and provide with complementary information (e.g., estimates of budget of biogenic elements, etc.).

Three-dimensional modeling exercises were also carried out to assess the interannual variability of the ecosystem dynamics in the NWMOS. *Bernardello et al*. [2012] showed a late onset of the bloom during cold winters compared to mild winters. The 30 year period modeling study of *Auger et al*. [2014] indicated a low interannual variability in yearly primary production which is not affected by winter mixing. They explained this finding by a seasonal balance between winter and spring primary production. Their results showed that a decrease in grazing might occur during strong mixing winters, due to prey rarefaction, resulting in an

unconstrained primary production during early spring. In contrast, these authors highlighted that during weak convection winters, the development of phytoplankton in winter and spring was more continuous. Based on a climatological modeling approach, *Herrmann et al*. [2013] showed that the export of organic matter is submitted to a large interannual variability mostly linked to the intensity of deep convection. Finally, results from *Bernardello et al*. [2012] indicated that the coupled-chronology of wind-mixing episodes and blooms is rather the most important factor which determines the intensity of yearly export fluxes. In this latter study, the winter export presents low interannual variability. However, it is noteworthy that these previous modeling studies were either restricted in time [*Bernardello et al*., 2012], based on a climatological approach [*Herrmann et al*., 2013], or only assessed a partial budget of organic carbon [*Auger et al*., 2014].

Hence, the objective of the present work is to estimate a global budget of organic carbon in the NWMOS at an annual scale, using a realistic approach. To that purpose, the interannual variability of the transport and biogeochemical fluxes of organic carbon, as well as of nutrients, in the NWMOS, was studied over a 5 year period (November 2003–2008) characterized by climatically contrasted winters, using a realistic high-resolution modeling approach. In particular, the exchanges between the photic zone and the deeper layer, as well as between the NWMOS and the adjacent shallow areas and open seas were assessed. The paper is organized as follows: section 2 describes the biogeochemical model and its coupling with an ocean circulation model. In sections 3 and 4, modeling results are presented and compared with in situ and satellite observations. An estimation of the main biogeochemical fluxes is performed in section 5. Finally, the main conclusions are given in section 6.

2. Material and Methods

2.1. The Coupled Physical-Biogeochemical Model

The modeling presented in this study is based on an offline coupling between a 3-D regional ocean circulation model and a biogeochemical model. Both models are described in the following sections.

2.1.1. The Hydrodynamic Model

We have used SYMPHONIE, a Boussinesq hydrostatic ocean circulation model developed by the SIROCCO group (http://sirocco.omp.obs-mip.fr). Momentum and tracer concentrations are computed on an Arakawa curvilinear C-grid using an energy conserving finite difference method described in *Marsaleix et al*. [2008]. The time stepping method consists of a Leap Frog scheme combined to a Laplacian filter [*Marsaleix et al*., 2012]. A generalized sigma coordinate is used in conjunction with a hybrid sigma/step method in area of steep topography in order to reduce the well-known "sigma coordinate errors" reported in *Auclair et al*. [2000]. A "pressure-Jacobian" method suited to the sigma coordinate is used to compute the pressure gradient scheme [*Marsaleix et al*., 2009, 2011]. The turbulence closure scheme consists of a prognostic equation for the turbulence kinetic energy combined to the mixing and dissipation length scales of *Gaspar et al*. [1990]. Radiative conditions are applied at the lateral open boundaries [*Marsaleix et al*., 2006] and combined with a restoring border layer toward the outputs of the general circulation model [*Estournel et al*., 2009]. Measured river discharges are introduced through a lateral volume and salt-conserving condition [*Reffray et al*., 2004].

This model was previously applied to study the formation of shelf dense water and its cascading over the slope [*Dufau-Julliand et al*., 2004; *Estournel et al*., 2005; *Ulses et al*., 2008], and the deep convection [*Herrmann et al*., 2008] in the NWMS.

2.1.2. The Biogeochemical Model

The biogeochemical model Eco3M-S described in details by *Herrmann* [2007] and *Auger et al*. [2011] represents the cycles of carbon (C), nitrogen (N), phosphorus (P), and silica (Si) and the dynamics of different plankton groups. Three size-classes of phytoplankton (pico, nano, and microphytoplankton), three size-classes of zooplankton (nano, micro, and mesozooplankton), and one class of bacteria are accounted for. The relative internal composition, i.e., the stoichiometry, is considered as variable for phytoplankton and constant for heterotroph organisms. Four compartments of dissolved inorganic nutrients (nitrate, ammonium, phosphate and silicate) are considered. Nitrate and ammonium are distinguished owing to their distinct roles in the functioning of pelagic ecosystem (new versus regenerated production). Phosphate is considered due to its important role in the control of the primary productivity at some periods of the year [*Diaz et al*., 2001; *Marty et al*., 2002; *Pasqueron de Fommervault et al*., 2015]. Dissolved organic matter (DOM) is considered in the model under the forms of C, N, and P. Particulate organic matter (POM, under the forms of C, N, P, Si, and chlorophyll) is divided into two weight classes, namely light and heavy. The food-web structure of the model and the

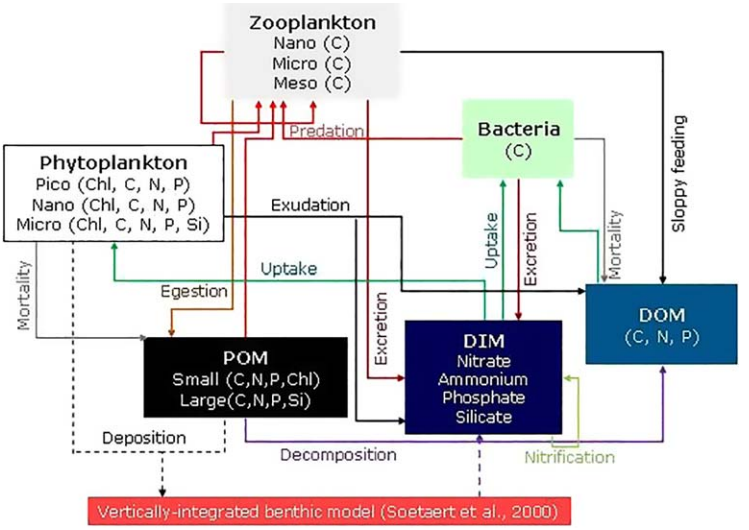

Figure 2. Scheme of the biogeochemical Eco3M-S model.

biogeochemical processes interacting between compartments are schematically represented in Figure 2. List of state variables is given in Appendix A Table A1.

The representation of the phytoplankton processes is derived from the model Eco3M presented and validated in *Baklouti et al.* [2006]. This model was extended to represent the various phytoplankton functional types computed in terms of carbon, nitrogen, phosphorus, silica (only for microphytoplankton), and chlorophyll contents with potential multinutrient limitation for their growth. The processes that drive the dynamics of development of phytoplankton functional types are (1) the gross primary production, (2) the autotrophic respiration, (3) the chlorophyll synthesis, (4) the exudation of dissolved organic carbon, (5) the uptake of nutrient, (6) the exudation of dissolved organic matter following the uptake of nutrients, and (7) the natural mortality (e.g., including viral lyses). The zooplankton and bacteria model is an adapted version of the stoichiometric model developed for heterotrophs by *Anderson and Pondaven* [2003] and applied in the Ligurian Sea by *Raick et al.* [2005]. The grazing, egestion, sloppy feeding, excretion, respiration, mortality, and predation by higher trophic level are the main processes driving the dynamic of zooplankton biomass at each time step in the model. The processes that drive the dynamics of the bacteria compartment are (1) the uptake of DOM and of nutrients, (2) the excretion of nutrients, (3) the respiration, and (4) the mortality. The process of decomposition of POM, represented in an implicit way, here stands for the hydrolysis activity of the particle-attached bacterial community. This process feeds DOM pool and silicates.

The model was used to study the interannual biogeochemical variability linked to atmospheric and hydrodynamic forcings from climatological [*Herrmann et al.*, 2013, 2014] and statistical [*Auger et al.*, 2014] points of view. For this study, a new calibration has been carried out to correctly capture the timing and intensity of spring blooms over the period 2004–2008 (Appendix A Table A2).

2.1.3. Implementation of the Coupled Model

A simulation with the hydrodynamic model has been first performed, storing daily-averaged currents, turbulent diffusion coefficient, and temperature. Then the biogeochemical model has been run with a 2 h time step, using the circulation model results as forcing fields.

We have used a regional-scale configuration on the western Mediterranean subbasin (0°40′W-11°40′E; 36°25′N-54°25′N, Figure 1) with 40 sigma-step vertical levels and a 2.5 km horizontal resolution, as described in *Auger et al.* [2014]. The model domain extent has been chosen to minimize the influence of boundaries in the area of interest, the NWMOS. The model has been run using initial and boundary conditions from the basin-scale OGCM NEMO-MED8 model with 1/8° resolution [*Herrmann et al.*, 2010]. For the atmospheric forcing, the daily outputs (radiative solar and long-wave fluxes, surface pressure, air temperature, relative humidity, and wind velocity) of the meteorological model ARPERA [*Herrmann and Somot*, 2008; *Herrmann et al.*, 2010], a downscaling of the ECMWF model reanalysis, was used. A relaxation term toward NEMO-MED8 daily sea surface temperature was applied with an 8 day restoring time scale for the heat flux. The water flux was the sum of the evaporation-minus-precipitation flux without any relaxation or correction, plus the river daily runoffs. Discharges of the most important river, the Rhône river, and of the Orb river have been prescribed using in situ daily data (sources: BANQUE HYDRO); discharges of Aude, Hérault, and Ebro rivers correspond to monthly climatological discharges calculated from, respectively, 9, 23, and 7 years of daily discharges (sources: BANQUE HYDRO and SAIH Ebro). The 5 year-averaged annual

Table 1. Five Year Average and Standard Deviation (std) of the Mean Annual River Discharges ($m^3\ s^{-1}$, Sources: BANQUE HYDRO for the French Rivers, and SAIH Ebro for the Spanish River) and Inorganic Nutrient Loads ($10^3 t\ yr^{-1}$)[a]

		Nutrient loads		
	Discharge	N	P	Si
Grand-Rhône	1290 (150)	68.8 (6.7)	1.85 (0.13)	92.5 (12.1)
Petit-Rhône	143 (17)	7.6 (0.7)	0.21 (0.01)	10.3 (1.3)
Hérault	51 (-)	1.1 (0.3)	0.03 (0.01)	1.4 (0.4)
Orb	23 (13)	0.7 (0.5)	0.02 (0.01)	0.9 (0.7)
Aude	30 (-)	1.7 (0.4)	0.04 (0.01)	2.3 (0.6)
Ebre	275 (-)	6.7 (1.4)	0.27 (0.07)	8.2 (2.2)

[a]Note that the 0 standard deviation corresponds to climatological values of the discharge.

discharge of the rivers is given in Table 1, and the temporal evolution of the discharges is presented in Appendix B Figure B1. The simulation starts in October 2003 and ends in November 2008.

For the initialization of the biogeochemical variables, we have used different sources of available data: to take into account the characteristics in nutrients of the different water masses of the region, we have initialized nitrate, phosphate, and silicate concentrations using density/nutrient relations obtained from observations collected during the DYNAPROC2 cruise, as performed by *Prieur and Legendre* [1988]. The initialization of the other state variables (bacteria, zooplankton, DOM, POM) has been done based on DYFAMED observations, when available, and literature data. Finally to obtain coherent biogeochemical variables, a preliminary simulation of the perpetual year 2004 has been performed. A quasi-steady state was reached after 2 years of simulation.

At each grid point of the open boundaries, the nutrient concentrations have been deduced from the density relation mentioned before and a zero-gradient condition has been applied for other variables.

Nitrate, ammonium, phosphate, and DOC concentrations have been prescribed at the Gulf of Lions river mouths using in situ monthly data (source: http://www.rdbrmc.com/cartordbrmc/) before March 2005, and daily data (http://mistrals.sedoo.fr/?editDatsId=767&datsId=767&project_name=MERMeX) from March 2005. Concentrations of silicate, DOP, DON, and POM have been estimated from these data and relations deduced from literature [*Moutin et al*., 1998; *Sempéré et al*., 2000] as described in *Auger et al*. [2011]. Table 1 gives the 5 year mean annual nutrients loads.

In order to take into account the fluxes of inorganic nutrients at the water-sediment interface, we coupled the pelagic model with a simplified version of the metamodel described by *Soetaert et al*. [2000]. In this version, key parameters (percentage of nitrification and of mineralization by denitrification) have been set to constant values according to the *Pastor et al*. [2011] study. Initial concentrations of the substances in the benthic model have been calculated by considering a steady state (equilibrium between deposition and mineralization processes) and are based on the 5 year averaged deposition fluxes. These latter fluxes have been obtained by an initial 5 year run of the pelagic model without coupling with the benthic model. Finally, atmospheric deposition of dissolved and particulate matter at the sea surface has been neglected and no flux induced by resuspension processes on the floor has been considered.

We focus in this study on the evaluation and analysis of the interannual variability of the hydrodynamic and biogeochemical fluxes and the annual budgets in the NWMOS. Therefore we have defined a "NWMOS box" as the area where depth is higher than 1500 m, delimited by longitudes 2°E and 9.5°E, and latitudes 40°N and 45°N (indicated in Figure 1), as in *Auger et al*. [2014], in order to compute averaged concentrations and fluxes. The delimitation by the 1500 m isobath was chosen (1) to include the areas of intense vertical mixing (winter mean mixed layer depth $>$ 200 m) and of bloom (surface chlorophyll concentration $>$ 1 mg m^{-3}) and (2) to avoid the signal of coastal processes. The delimitation in longitudes and latitudes was set to include the bloom areas as defined by *D'Ortenzio and Ribera d'Alcala* [2009] and *Bernardello et al*. [2012]. A sensitivity study to the choice of the "box" boundaries on the various fluxes and budget terms is presented in section 5.3.4. The annual fluxes and budgets have been computed from November to November in order to include the preconditioning phase of open-sea convection events.

2.2. Data Used for the Model Evaluation

In order to evaluate the quality of the coupled model outputs we have used a set of in situ and remotely sensed observations over the study period.

The sea surface temperature (SST) of the hydrodynamic model was compared to NOAA AVHRR satellite data downloaded from the EOWEB Geoportal of DLR (http://eoweb.dlr.de).

The DYFAMED station is located in the central part of the Ligurian Sea, offshore the Cap Ferrat, at 2350 m deep (Figure 1). In the framework of the JGOFS program, long time series of hydrological and biogeochemical parameters were collected, from 1991 until now (doi:10.12770/271cddd7-e9af-4175-9398-3f3e272af9bb), with the aim to study the seasonal and decadal variations, and the potential response of the ocean to anthropogenic and climate perturbations. These data were analyzed notably for phytoplankton by *Marty et al*. [2002] and *Marty and Chiavérini* [2010], for heterotrophs by *Tanaka and Rassoulzadegan* [2002], as well as by *Miquel et al*. [2011] for the export of detritus material and by *Pasqueron de Fommervault et al*. [2015] for nutrients. In order to validate the vertical structure of the biogeochemical model outputs, we have collected the available observations from October 2003 to July 2007: monthly profiles of the chlorophyll pigments, nutrients, and bacteria abundance. The DYFAMED time series of chlorophyll pigments has been completed with the Bousssole project data [*Antoine et al*., 2006, 2008] from September 2007 to November 2008. We have used the relation established by *Uitz et al*. [2006] to deduce from pigments the chlorophyll concentrations of the three modeled size classes of phytoplankton (pico, nano, and microphytoplanktons). An evaluation of the orders of magnitude and seasonal variations of modeled variables that were not observed during the study period has been finally done with previous observations (for instance for heterotrophs, we have referred to the observations reported by *Tanaka and Rassoulzadegan* [2002]).

We have also collected daily images of chlorophyll a concentration from sensor Aqua-MODIS (http://disc.sci.gsfc.nasa.gov/giovanni) from November 2003 to November 2008 in order to validate the time and spatial patterns of surface chlorophyll-a concentration. The data have been interpolated on the model grid for comparisons with model results. Monthly-mean modeled surface chlorophyll maps have been computed using outputs for the dates and locations for which satellite data were available.

3. Meteorological and Hydrodynamic Context in the North-Western Mediterranean Open Sea From 2003–2004 to 2007–2008

In this section, the atmospheric and hydrodynamic conditions, as well as their interannual variability, are presented and checked against observations that were mostly collected during the study period.

3.1. Heat Fluxes

Figure 3a presents the seasonal time series of the modeled air-sea heat fluxes averaged on the NWMOS. Heat fluxes generally present negative values (loss from the ocean to the atmosphere) from September to March. The mean winter heat loss is maximum in winter 2004–2005 (winter: 1 November to 15 March, 235 W m^{-2}), which was reported by *Lopez-Jurado et al*. [2005] as an exceptionally cold and dry winter. It is minimum in winter 2006–2007 (125 W m^{-2}). Moreover, one can notice that in winter 2004–2005 strong heat loss episodes are very frequent (four episodes where the mean heat loss is higher than 300 W m^{-2}) relative to the other years and the heat loss remains higher than 200 W m^{-2} until mid-March. The study period is thus characterized by contrasted winters submitted to heat loss events of variable intensity.

3.2. Winter Vertical Mixing

Figure 3b displays the temporal evolution of the model estimate of the Mixed Layer Depth (hereafter MLD) averaged on the NWMOS. The MLD has been defined here as the depth until which the daily averaged vertical diffusivity is smaller than 4.10^{-4} m^2 s^{-1} [*Herrmann et al*., 2008; *Auger et al*., 2014]. For each year, (1) the MLD increases in November, (2) the spatially averaged maximum is reached in March, and (3) the water column abruptly restratifies in mid-March. This modeled seasonal pattern fairly agrees with the climatology results of previous observational studies [*D'Ortenzio et al*., 2005; *Marty and Chiavérini*, 2010; *Heimbürger et al*., 2013], using a MLD calculation based on temperature and salinity in situ profiles, with a potential density criterion based on a difference of 0.03 kg m^{-3} from a near-surface value at 10 m depth [*D'Ortenzio et al*., 2005]. Note that the seasonal variation of the MLD model estimate based on this method is similar to the one obtained with a criterion on a threshold on the vertical diffusivity (not shown). Beyond this general seasonal pattern, the amplitude of the MLD presents an important interannual variability, mainly driven by atmospheric forcing. The maximum of the MLD averaged over the NWMOS box varies between 497 m in 2004–2005 and 78 m in 2006–2007 in the model. Figure 3b indicates that the vertical mixing is much

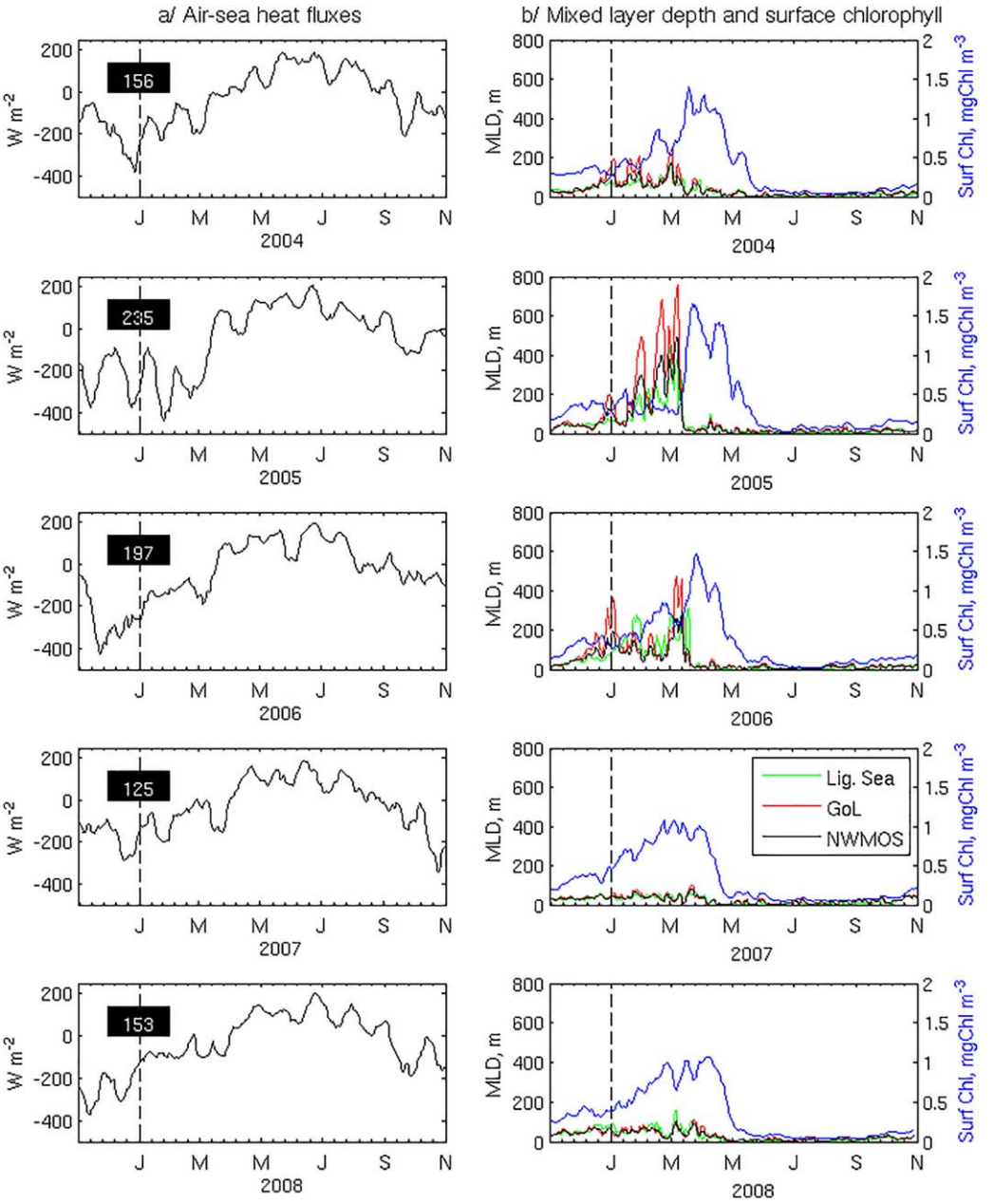

Figure 3. Time series of modeled (a) air-sea heat fluxes (W m^{-2}) averaged on the NWMOS box (value of the spatial mean winter (1 November to 15 March) total heat loss is indicated in black rectangles), and (b) mixed layer depth (m) averaged on the NWMOS box (in black), the MEDOC box (in red), and the Ligure box (in green) and surface chlorophyll concentration (mg m^{-3}) averaged over the NWMOS box (in blue). The NWMOS, MEDOC, and Ligure boxes are indicated on Figure 1.

deeper in the Gulf of Lions than in the Ligurian Sea, except at certain periods as January, February, and March 2006. A significant correlation (0.71, $p < 0.01$) was obtained between the model estimate and the estimate deduced from monthly observations at the DYFAMED station, that partly capture the interannual variability [*Marty et al*., 2002; *Marty and Chiavérini*, 2010; *Miquel et al*., 2011; *Pasqueron de Fommervault et al*., 2015]. In this comparison, both model and observational MLD estimates were calculated using the method based on density criterion.

Figure 4a presents for each year a composite map for which each pixel corresponds to the thickest MLD modeled during the winter. Although the maximum convection area is located offshore the Gulf of Lions over the five winters, the extent of the vertical mixing, as well as its intensity, clearly show a high interannual variability.

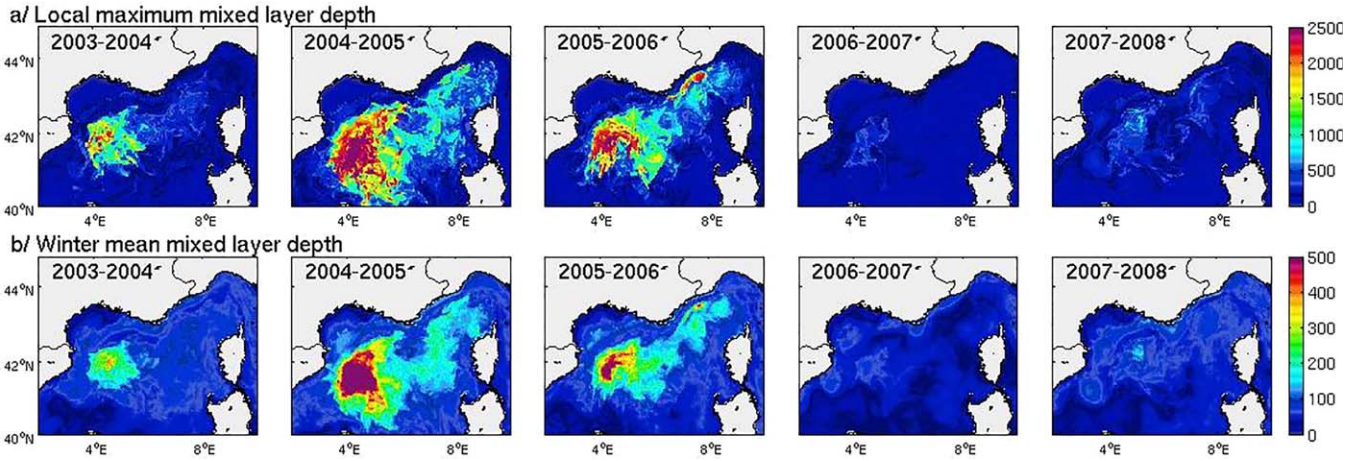

Figure 4. (a) Local maximum mixed layer depth (m) and (b) mean winter mixed layer depth (m) simulated for year 2003–2004 to year 2007–2008.

In winter 2003–2004, the NWMOS spatially averaged MLD varies between 50 and 150 m from January to March (Figure 3b). The model results indicate that deep convection occurs first offshore the Gulf of Lions where it reaches 2000 m from the end of January–March (not shown). Vertical mixing locally beyond 400 m depth is also modeled in mid-March in the Ligurian Sea.

In winter 2004–2005, five successive episodes of intense northern wind associated to strong heat loss events from December to early March (Figure 3a) induce a progressive deepening of the ML, with the NWMOS spatial average reaching 500 m in early March (Figure 3b). More locally, the MLD reaches the bottom in the MEDOC area, located around 42°N–5°E [*MEDOC Group*, 1970], at the end of January. The water column finally restratifies in mid-March in agreement with *Herrmann et al*. [2010] model results. During winter 2004–2005, the deep convection area clearly extends westward, in the Balearic Sea, and southward (Figure 4). This is consistent with *Font et al*. [2007] CTD observations South of the Palamos Canyon and with Argo floats observations reported by *Smith et al*. [2008] showing a deep convection up to 2000 m at the North-East of the Balearic Islands (39.785°N; 4.845°E). The modeling results show an area of convection beyond 1700 m depth at the same period near the location of the Argo float. In the Ligurian Sea, the modeled MLD reaches 2000 m in the frontal area along the Northern Current and varies episodically between 700 and 1000 m in mesoscale structures.

In winter 2005–2006, two episodes of heat loss in January and then in March (Figure 3a) induce two strong events of violent vertical mixing (Figure 3b). Deep convection takes place in the MEDOC area in early January and March; in the Ligurian Sea it takes place at the end of January, in February, and in March. Vertical mixing reaches the bottom in both areas alternatively. The largest vertical mixing in the Ligurian Sea is located along the Northern Current, as in winter 2004–2005, but is deeper and, spatially and temporally more extended than during the previous winter (Figure 4). These modeling results are again consistent with Argo float observations reported by *Smith et al*. [2008]: Argo float 292 was located in the MEDOC area in February between the two strong convection events and therefore it did not register strong mixing. In contrast, Argo float 293 was located in February and March, in the Ligurian Sea where it recorded uniform profiles of density; its trajectory was in the core of the deep convection as simulated by the model (Figure 4a). The model outputs are also in agreement with the results of *Pasqueron de Fommervault et al*. [2015] who reported values greater than 2000 m, observed for the first time at the DYFAMED station.

During both following winters, 2006–2007 and 2007–2008, vertical mixing is globally quite weak (Figure 4). The NWMOS spatial mean MLD does not deepen beyond 100 m (Figures 3b). In winter 2006–2007, the maximum MLD is shallower than 600 m and vertical mixing is restricted to the MEDOC region (Figure 4a). In winter 2007–2008, the vertical mixing extends in the Ligurian Sea and the maximum MLD reaches 600 m in the Ligurian Sea and 900 m in the MEDOC area (Figure 4a). This is in agreement with temperature profiles collected at the LION buoy (located at 42°2.5′ N, 4°41′ E, at 2350 m depth, Figure 1) and reported by *Stabholz et al*. [2013].

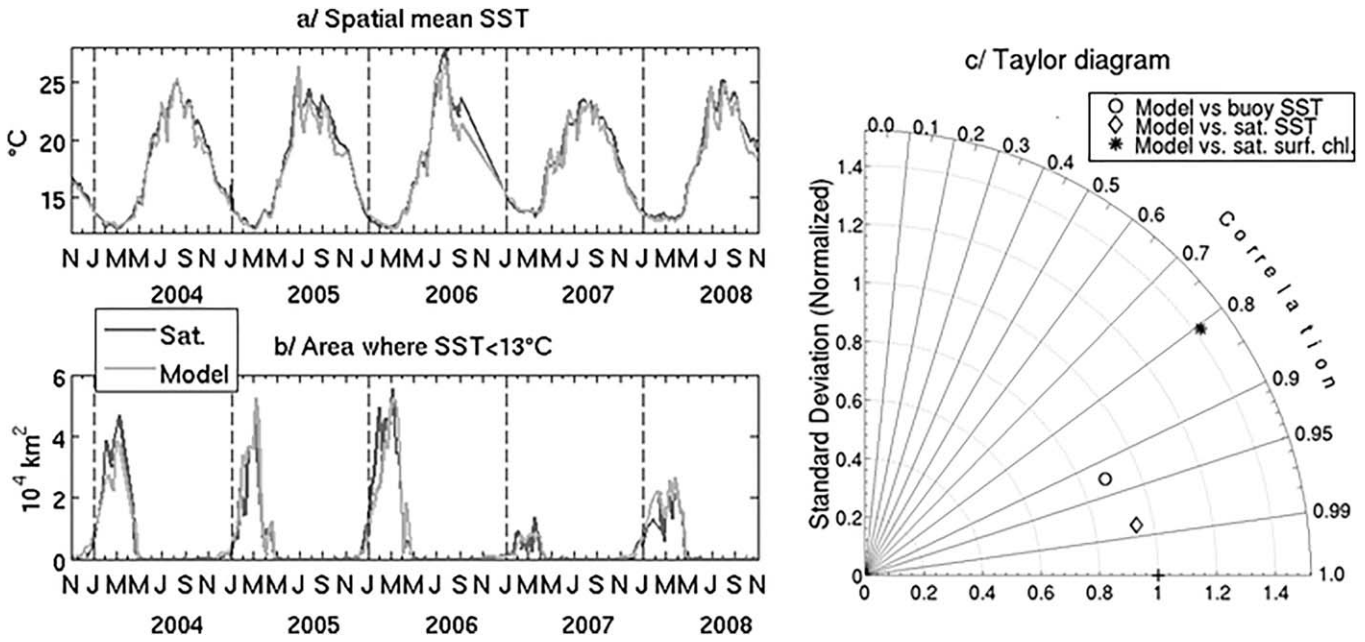

Figure 5. Time evolution of (a) spatially averaged SST (°C) and (b) the extension of the area where SST is less than 13 °C (10^4 km^2), in the NWMOS, in satellite data (dark grey), and in the model results (light grey); (c) Taylor diagram: radius is normalized standard deviation and angle is correlation. The black cross indicates a perfect match between model and observations. The diagram gathers the comparisons of the model results with the SST satellite data (diamond), the SST LION buoy data (circle), and the satellite chlorophyll data (asterisk).

3.3. Sea Surface Temperature

Figures 5a and 5b present, respectively, the time evolution of SST averaged over the NWMOS, and the time evolution of the surface of the NWMOS-included area where SST is smaller than 13°C, both for model outputs and satellite data. The model correctly simulates the evolution of the mean SST; in particular, during winter, the SST minimums are accurately represented both in time and magnitude. Hence the model interannual variability of the annual SST minimum is very coherent with the one associated with the observations: indeed in both signals, the SST minimum is smaller than 12.5°C in 2004, 2005, and 2006, and of the order of 13°C in 2007 and 2008. Besides, the evolution and the interannual variability of the spatial extension of low SST (<13°C) waters are also well reproduced by the model. This spatial extension reaches about 10^4 km^2 during the 2007 mild winter and 5 10^4 km^2 during 2005 and 2006 cold winters. The *Taylor* diagram [*Taylor*, 2001] (Figure 5c) shows a significant correlation coefficient of 0.98 ($p < 0.01$) between satellite data and modeled SST and a slightly smaller normalized standard deviation in the model.

The modeled SST has also been compared to the SST measured at the LION buoy (http://data.datacite.org/10.6096/HyMeX.LionBuoy.Thermosalinograph.20100308, not shown). This comparison led to a significant correlation of 0.93 ($p < 0.01$) and a smaller standard deviation of 15% for the model results (Figure 5c).

Finally the *Nash-Sutcliffe* efficiency coefficient [*Nash and Sutcliffe*, 1970] has been calculated. It also reflects a realistic representation of the physical properties in the model results as it reaches 0.96 for the comparison with satellite data and 0.86 for the comparison with in situ data.

4. Spatial and Temporal Biogeochemical Variability of the NWMOS

We show in the following section a set of comparisons between biogeochemical model results and available observations over the study period, listed in section 2.2. These comparisons enable us to evaluate the ability of the model to represent the main biogeochemical characteristics of the studied area and period. We focus here on the seasonal and interannual variations of the ecosystem dynamics, in the NWMOS area.

4.1. Surface Chlorophyll

We have compared modeled surface chlorophyll concentrations, averaged over the NWMOS area, with MODIS satellite images, over the period 2004–2008. Figure 6a displays the time series of both modeled and observed surface chlorophyll concentrations. Model results globally fit quite well with the satellite data. The onset of the

spring blooms and their duration are generally correctly simulated by the model. Nevertheless, the increase in chlorophyll concentration in winter is higher in the model. This difference could be due to an overestimation of primary production in the model and/or to an underestimation by satellite algorithm in winter [*Gernez*, 2009]. Finally, from June to September, the modeled chlorophyll is slightly higher than the observed one. This difference could be attributed to an underestimation of the satellite data as shown by *Bosc et al*. [2004] through comparisons with DYFAMED in situ data. A temporal-mean RMS error of the spatially averaged surface chlorophyll of 0.23 mg m^{-3} and a correlation coefficient of 0.80 ($p < 0.01$, Figure 5c) confirm a satisfying global agreement between model results and observations. The model results come with a standard deviation 42% greater than the one associated with the observations (Figure 5c). Moreover, the time correlation coefficient has been calculated at each grid point (not shown). It mostly varies between 0.5 and 0.9, and is always significant ($p < 0.05$). As obtained by *Auger et al*. [2014], the lowest correlations have been found in the area of important submesoscale activity (slope and convective regions). Finally, the value of the *Nash-Sutcliffe* efficiency coefficient is 0.26, reflecting a correct agreement between model outputs and satellite data.

Figure 3b presents the cycles for both simulated surface chlorophyll and MLD averaged on the NWMOS from November 2003 to November 2008. During years 2003–2004, 2004–2005, and 2005–2006, the MLD strongly deepens from January to March as previously mentioned. During the mixing events, the surface chlorophyll decreases likely due to wind-induced dilution over the water column. After a sudden restratification in early/mid-March, surface chlorophyll concentration abruptly increases. The date of the maximum MLD is, respectively, 33, 25, and 19 days before the date of the maximum surface chlorophyll for years 2003–2004, 2004–2005, and 2005–2006. The cycles of surface chlorophyll and MLD are notably different for years 2006–2007 and 2007–2008, when the winter mixing is globally weak. The surface chlorophyll concentration almost constantly increases from January to mid-March for 2006–2007 and to early April for 2007–2008. During this period, small decreases in surface chlorophyll are nevertheless visible when weak and brief vertical mixing episodes occur. Contrary to years 2003–2004, 2004–2005, and 2005–2006, the maximum of surface chlorophyll in 2006–2007 is preceding the maximum of MLD, by 5 days. Finally, one can notice that the interannual variability of the surface chlorophyll annual maxima (mean: 1.3 mg m^{-3}, std: 0.2 mg m^{-3}) is clearly smaller than the one of MLD (mean: 229 m, std: 171 m). Same interannual variability in the cycles of MLD and surface chlorophyll, with a similar anomaly in 2006–2007, was found by *Lavigne et al*. [2013] for the "Bloom North-West" bioregion based on in situ temperature and salinity profiles as well as MODIS and Seawifs surface chlorophyll data.

The spatial distributions of simulated surface chlorophyll and satellite MODIS observations are visible on Figures 6b and 6c. We have chosen to present here an average on April, the month when the spring bloom is generally the most intense. The spatial extension and intensity of the spring bloom are correctly captured by the model in the NWMOS. For April 2008, the model estimates are lower than those of the satellite data, but the location of the maximum of surface chlorophyll concentration in the Ligurian Sea is well reproduced. The underestimation default could be attributed to a too smooth and weak vertical mixing in the model.

4.2. Biogeochemical Vertical Structure

Figure 7 displays a comparison between observed and modeled vertical profiles of chlorophyll, nutrients, and bacteria concentrations at the DYFAMED deep station at the same days. We have chosen to present here a comparison by season to assess the ability of the model to represent an annual cycle. This comparison is completed with the RMS error computed over the whole study period (Figure 8).

In winter, the model correctly reproduces the weak concentrations of chlorophyll for the three phytoplankton groups in the homogenized upper layers (0–200 m) (Figure 7). The concentration of nitrate and silicate in surface and intermediate waters is slightly underestimated in winter by the model, whereas the simulated phosphate concentration stands within the range of observed values. In spring, the model satisfyingly reproduces the increase of chlorophyll in the 0–50 m surface layer. In summer, it simulates, in agreement with observations, a deepening of the chlorophyll maximum due to the nutrient depletion in the surface layers. Finally, in fall the homogenization of the surface layer concentration provoked by an intensification of wind in November and December is correctly reproduced by the model. On the whole period, the integrated chlorophyll content for the three phytoplankton groups is distributed as follows: micro: 33%, nano: 52%, and pico: 15%. These modeled contributions of phytoplankton groups are consistent with the one obtained by *Marty and Chiavérini* [2010] who measured over the 1991–2007 DYFAMED data set the

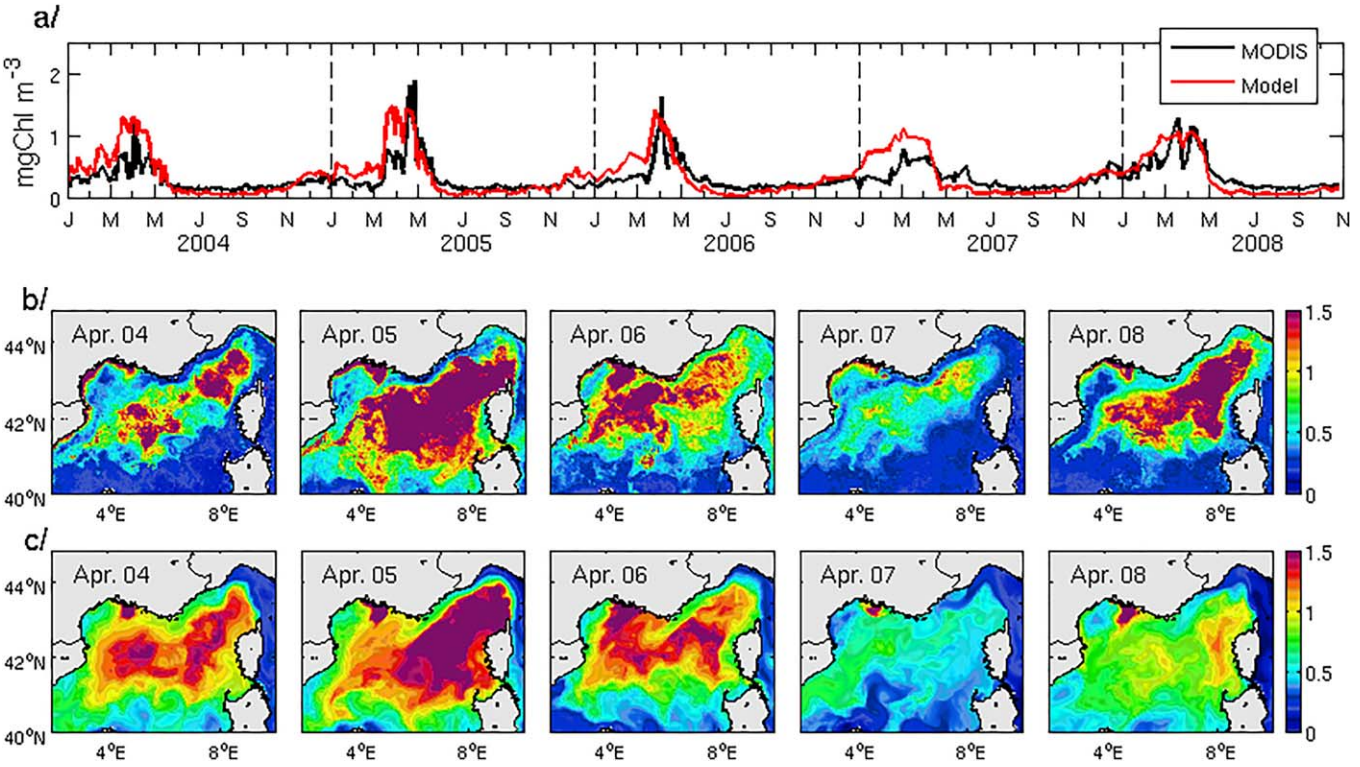

Figure 6. (a) Time series of modeled (in red) and observed by MODIS satellite (in black) surface chlorophyll-a concentration (mg m^{-3}) averaged over the NWMOS from January 2004 to November 2008; (b) observed by MODIS satellite and (c) modeled April averaged surface chlorophyll-a concentration for 2004–2008.

following distribution: micro: 37%, nano: 45%, and pico: 18%. The microphytoplankton generally dominates during the bloom period, while the nanophytoplankton dominates the rest of the year (not shown), in agreement with *Marty and Chiavérini* [2010] observations.

Concerning bacteria concentration, the model simulates, in agreement with measurements, low and homogeneous concentrations in winter, an increase in the surface layer in spring and a persistence of the biomass maximum depth in summer. However, one can notice that the model underestimates the decrease in concentrations during fall.

These comparisons show that the model is able to capture quite correctly the observed seasonal cycle of the vertical profiles of chlorophyll, nutrients, and bacteria. The orders of magnitude of the variables and the repartition of the three phytoplankton groups simulated by the model are in reasonable agreement with in situ measurements.

The profiles of the time-averaged RMS errors for the concentration of chlorophyll, nutrients, and bacteria over the period 2004–2008 are presented in Figure 8a. The maximal RMS error for the three phytoplankton groups and bacteria is located in the first 50 m, where the associated concentrations and the vertical gradients are the largest. The RMS error is found to be about 0.2 and 0.3 mgChl m^{-3} for the dominant groups, respectively, micro and nanophytoplankton, and lower than 0.1 mgChl m^{-3} for picophytoplankton. The time-averaged RMS error is smaller than 0.5 mmolC m^{-3} for bacteria, 2 mmol m^{-3} for nitrate and silicate, and 0.07 mmol m^{-3} for phosphate.

The depth-averaged RMS error associated with chlorophyll concentrations is relatively low from January to early March, when the concentrations are small (Figure 8b), except in 2008 when the model underestimates an early bloom. The larger depth-averaged RMS errors are generally visible during spring bloom periods, in particular in April 2006 when the model underestimates an increase in microphytoplankton biomass. The depth-averaged RMS error for phosphate is smaller than 0.2 mmol m^{-3}, while these errors for nitrate and silicate are found to be around 2 mmol m^{-3}. Finally the depth-averaged RMS error for bacteria is below 0.5 mmol m^{-3}, except in April 2004 when the model overestimates the in situ measurements.

Since no data were available for zooplankton and DOC concentrations on the study period, we have confronted the simulation results for these variables to literature data. The nano and microzooplankton

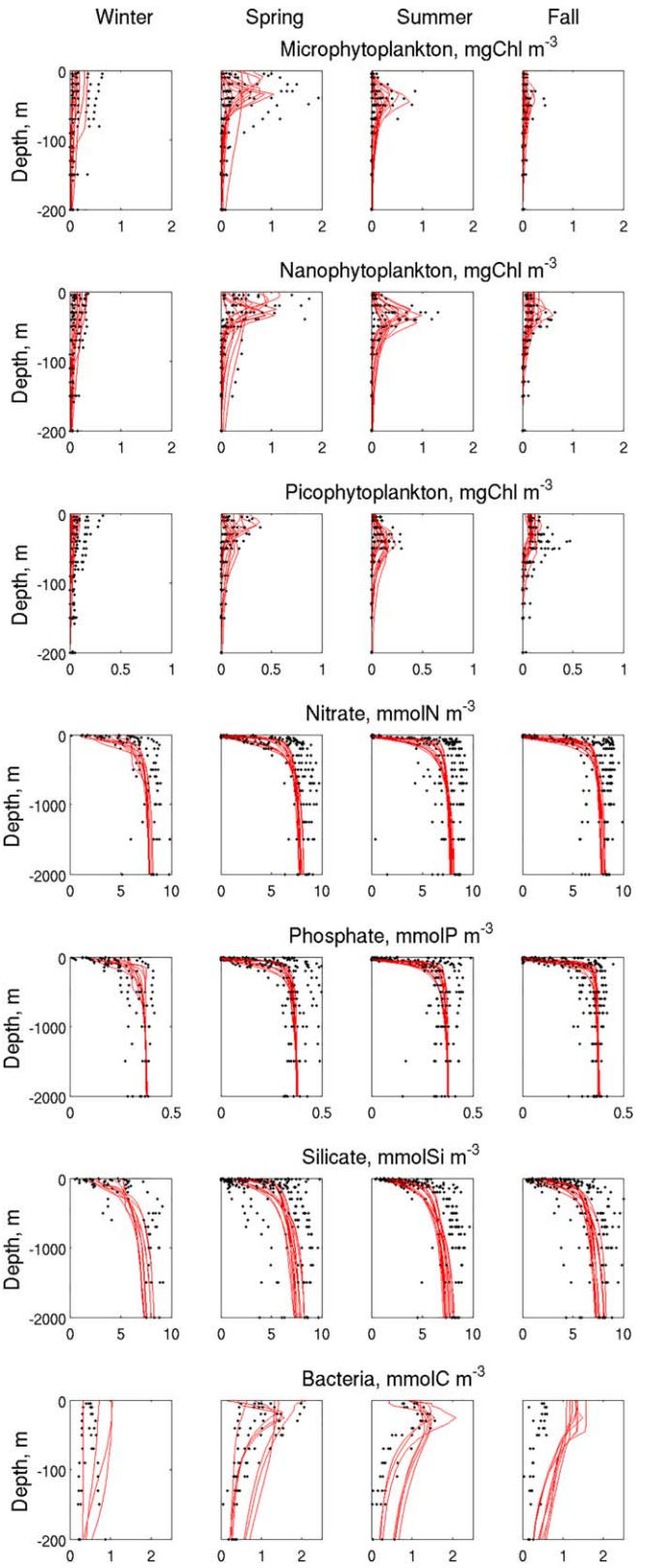

Figure 7. Comparison between observed (black points) and simulated (red lines) profiles of chlorophyll concentration (mg m^{-3}) associated to the three phytoplankton size-classes and of nitrate, phosphate, silicate, and bacteria concentrations (mmol m^{-3}), by season (winter: 21 December to 20 March, spring: 21 March to 20 June, summer: 21 June to 22 September, fall: 23 September to 20 December), at the DYFAMED station.

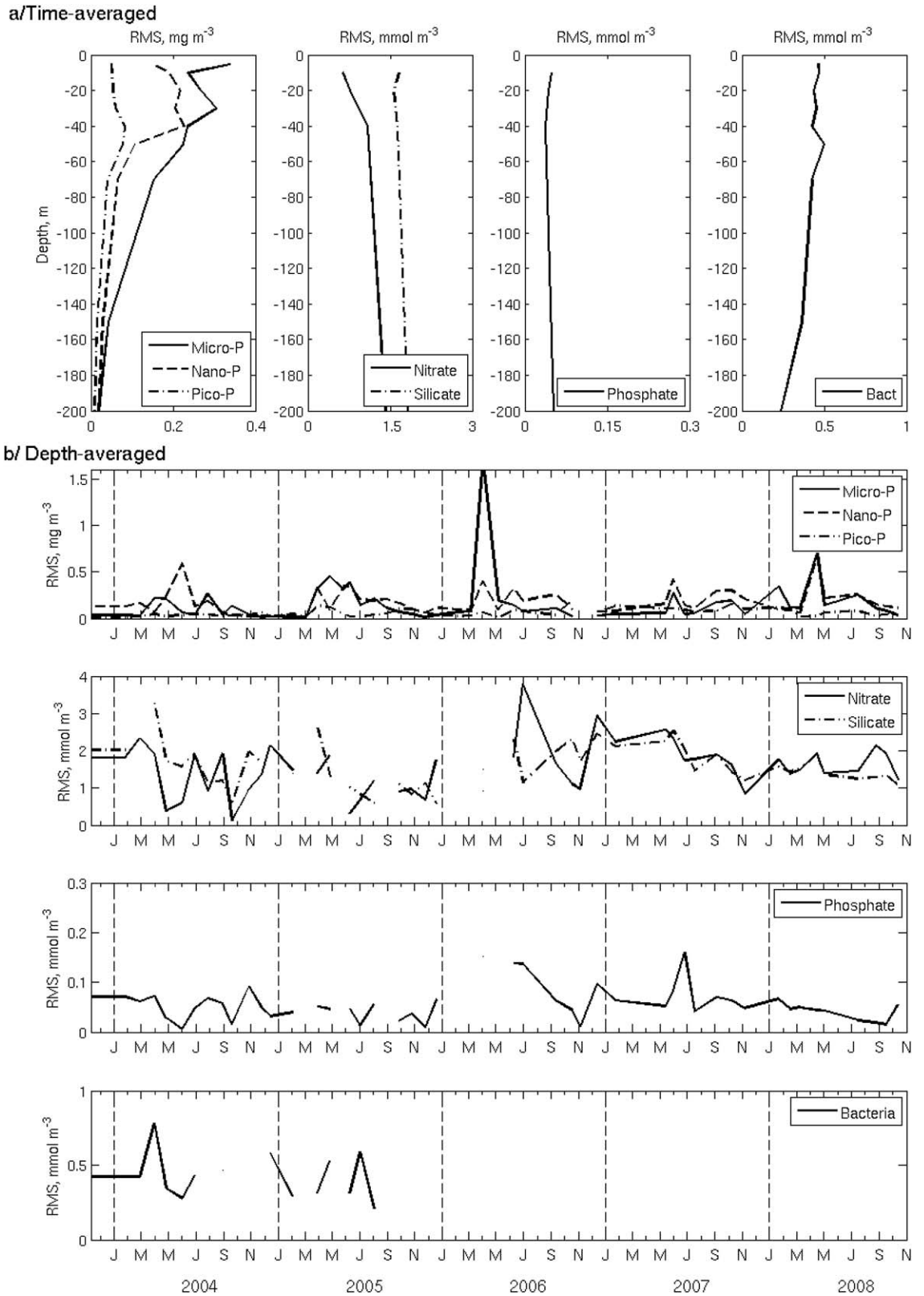

Figure 8. (a) Time-averaged and (b) depth-averaged RMS error for the concentrations of chlorophyll-a (mg m^{-3}) for the three phytoplankton size-classes, nutrients (mmol m^{-3}), and bacteria (mmolC m^{-3}) from November 2003 to November 2008 at the DYFAMED station. DYFAMED data have been used from November 2003 to July 2007 and Boussole project data have been used from September 2007 to November 2008.

biomasses, integrated over the 0–110 m surface layer simulated at the DYFAMED station, range, respectively, between 0 and 30 mmolC m^{-3}, and 0 and 55 mmolC m^{-3} over the whole study period. They present the same order of magnitude as observations by *Tanaka and Rassoulzadegan* [2002], ranging, respectively, between 1.4 and 20 mmolC m^{-3} and 3.7 and 51 mmolC m^{-3}.

The modeled semilabile DOC concentration in the NWMOS is homogeneous from January to March during the vertical mixing periods (not shown). In spring, it increases during the bloom, especially in the first 50 m. It is higher than 20 mmolC m^{-3} in the 50 m surface layer and decreases to ~7 mmolC m^{-3} at 100 m. It reaches 40 mmolC m^{-3} during stratified periods following intense deep convection events. High concentrations persist until December before the vertical mixing intensifies. Those values are close to the concentrations observed by *Santinelli et al.* [2010] and *Avril* [2002] during the stratification period, ranging between 30 and 45 mmolC m^{-3} at the surface (if 50 mmolC m^{-3} is substracted for the refractory part). They are lower than the concentrations observed by *Avril* [2002] during the winter mixing period at the DYFAMED site, ranging between 20 and 30 mmolC m^{-3} at the surface (in the model at this site minimum values are around 5 mmolC m^{-3} each year, except during the 2007 mild winter when they are around 10 mmolC m^{-3}). The latter observations took place from 1991 to 1993, a period characterized by shallow winter mixing [*Auger et al.*, 2014] that could have led to a small export of dissolved organic matter from the surface layer to the underlying waters. Nevertheless our results are consistent with recent observations from DEWEX1 survey taking place in February 2013 where homogeneous DOC profiles were recorded at stations located in deep convection areas in the Gulf of Lions and in the Ligurian Sea (M. Pujo-Pay, personal communication, 2015).

5. Budget in the NWMOS

In the following sections, we present the model-derived time evolution and budget estimates of the volume of dense water (section 5.1), of the upward fluxes of nutrients into the surface layer (section 5.2), and of the fluxes of organic carbon (section 5.3), in the NWMOS. These model results are compared with previous

Table 2. Amount of Dense Water Formed at the Surface by Atmospheric Fluxes, Amount of Nutrients Injected Into the Surface Layer in Winter (21 December to 20 March; When Positive, Net Upward Import; When Negative, Net Downward Export) and Biogeochemical Fluxes (Annual Gross and Net Primary Production, Winter and Spring Gross Primary Production; Downward Export Flux of Particulate and Dissolved Organic Carbon at 100 m Depth, Export Flux of Particulate Organic Carbon at 1000 m Depth and Near the Bottom; Ratio Between the Export Flux of POC at 100 m, 1000 m and Near the Bottom, and the GPP) for Year 2003–2004 to Year 2007–2008 and Averaged on the 5 Year Period, Estimated From the Model

		Unit	2003–2004	2004–2005	2005–2006	2006–2007	2007–2008	Mean (std)[a]
Cumulated dense water formed at the surface by atmospheric fluxes		10^{13} m^3	1.6	7.8	5.2	0	0.2	3.0 (3.4)
Amount of Nutrients Injected Into the Surface Layer (0–100 m) in Winter	NO_3	10^3 tN	445	1222	641	−136	276	490 (500)
	PO_4	10^3 tP	34	117	67	−29	19	42 (54)
	SiO_2	10^3 tSi	525	1840	708	−208	382	650 (749)
Annual GPP[b]		**gC m^{-2} y^{-1}**	**275**	**286**	**282**	**289**	**281**	**283 (5)**
Winter GPP		**gC m^{-2} y^{-1}**	182	158	180	231	212	**193 (29)**
Spring GPP		**gC m^{-2} y^{-1}**	399	454	421	367	376	**403 (35)**
Annual NPP[c]		**gC m^{-2} y^{-1}**	148	148	148	154	151	**150 (3)**
POC[d] export at 100 m		**gC m^{-2} y^{-1}**	**26.7**	**36.0**	**31.2**	**18.6**	**24.7**	**27.4 (6.6)**
% Sedimentation		**%**	27	20	21	34	30	**26 (6)**
% Advection		**%**	69	66	68	65	68	**67 (2)**
% Turbulence		**%**	5	13	11	1	2	**6 (6)**
POC export/GPP at 100 m		**%**	**10**	**13**	**11**	**6**	**9**	**10 (2)**
DOC[e] export at 100 m depth		**gC m^{-2} y^{-1}**	**14.4**	**20.1**	**18.1**	**11.3**	**12.1**	**15.2 (3.8)**
POC export at 1000 m		**gC m^{-2} y^{-1}**	**3.6**	**6.7**	**5.0**	**2.8**	**3.2**	**4.3 (1.6)**
% Sedimentation		**%**	77	46	52	90	89	**71 (21)**
% Advection		**%**	22	53	47	10	10	**29 (21)**
% Turbulence		**%**	0	1	1	0	0	**1 (1)**
POC export/GPP at 1000 m		**%**	**1**	**2**	**2**	**1**	**1**	**2 (1)**
POC deposition		**gC m^{-2} y^{-1}**	**2.3**	**2.6**	**2.2**	**2.1**	**2.4**	**2.3 (0.2)**
POC dep.[f]/GPP		**%**	0.9	0.9	0.8	0.7	0.9	**0.8 (0.1)**

[a]std: standard deviation, [b]GPP: gross primary production, [c]NPP: net primary production, [d]POC: particulate organic carbon, [e]DOC: dissolved organic carbon, [f]dep.: deposition.

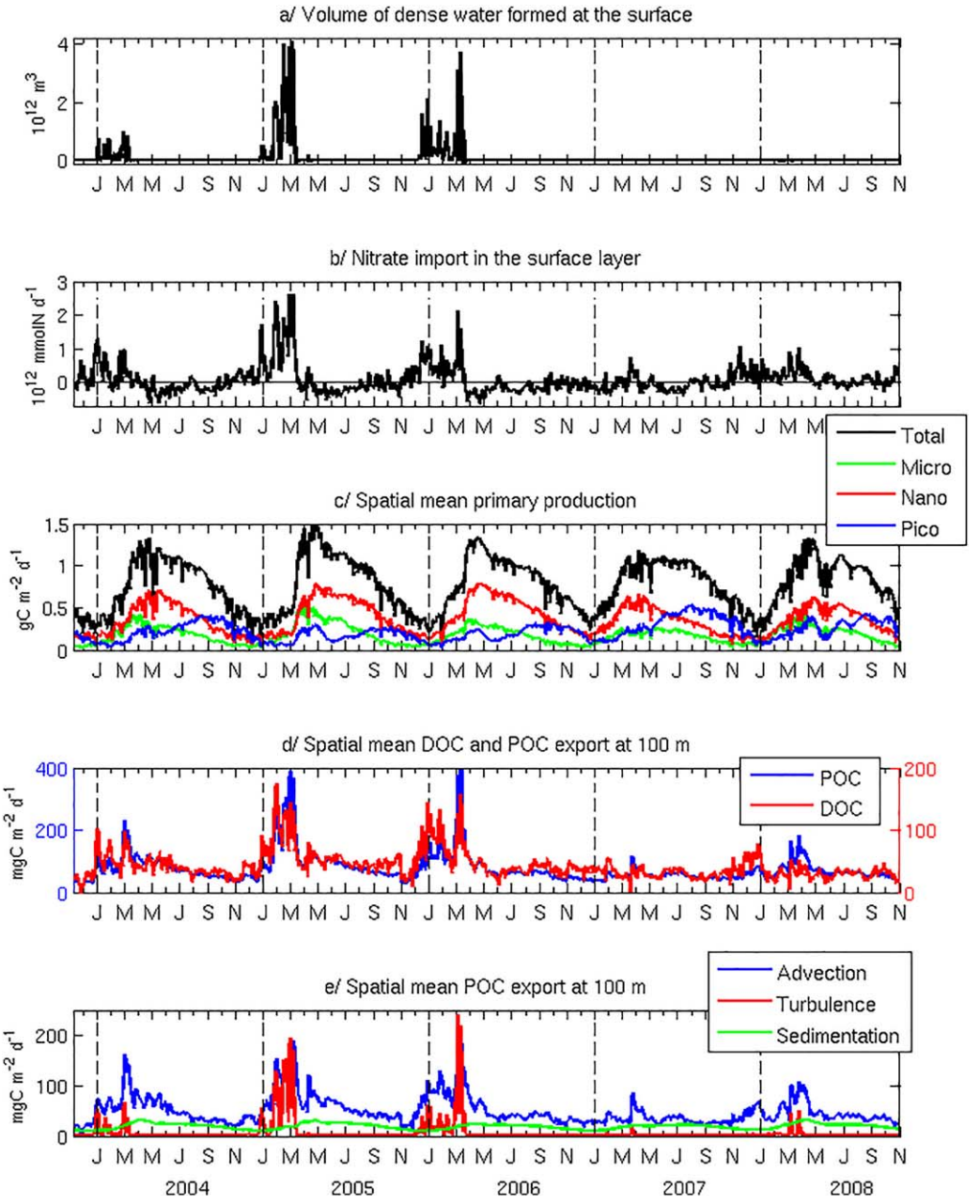

Figure 9. (a) Volume of dense water (10^{12} m^3) formed at the surface due to atmospheric fluxes, (b) transport of nitrate (10^{12} mmolN d^{-1}) into the surface layer calculated at 100 m depth (when positive net upward import; when negative net downward export), (c) spatial mean gross primary productions (gC m^{-2} d^{-1}), (d) spatial mean export fluxes of POC and DOC (mgC m^{-2} d^{-1}) and (e) spatial mean POC export flux (mgC m^{-2} d^{-1}) by advection (in blue), turbulent mixing (in red), and sedimentation (in green), over the NWMOS. POC: particulate organic carbon, DOC: dissolved organic carbon.

studies. In section 5.3, a global budget of organic carbon and its sensitivity to the analysis domain boundaries are presented, following an assessment of the primary production and the downward export.

5.1. Dense Water Formation

Figure 9a presents the time evolution of the volume of dense water driven by atmospheric fluxes. We have computed this volume using the method of *Walin* [1982]. The critical density has been set to 1029.1 kg m^{-3}. From winter 2003–2004 to winter 2005–2006, the volume of the formed dense water follows a similar evolution to the one of the MLD (Figure 3b). It is null or very small in winters 2006–2007 and 2007–2008. The cumulative volume formed for each studied year is indicated in Table 2. It reaches 1.6 10^{13} m^3, 7.8 10^{13}

m^3, and 5.2 10^{13} m^3, respectively, in winters 2003–2004, 2004–2005, and 2005–2006. Our estimates are in the same order of magnitude as the ones calculated by *Herrmann et al*. [2008] and [2010] who found volumes of 4.6 10^{13} m^3 and 3.7 10^{13} m^3, respectively, in winters 1986–1987 and 2004–2005, also using 3-D modeling approaches. Our results are also consistent with the volume given by *Durrieu de Madron et al*. [2013] of 2.5 10^{13} m^3 for winter 2011–2012 using multiplatform observations, and very close to the results of *Schroeder et al*. [2008] who estimated a total mean production rate of 15 10^{13} m^3 for a period including both winters 2004–2005 and 2005–2006, based on CTD observations.

5.2. Vertical Import of Nutrients Into the Surface Layer

The time evolution of the amount of nitrate entrained into the surface layer (0–100 m) in the NWMOS through advection and turbulent mixing is reported in Figure 9b. The upward transport exhibits clearly a seasonal signal with maxima between November and March/April. During this period, violent wind events occur and the surface waters are mixed (Figure 3) with nutrient-rich deep water masses. We found an 80% significant correlation ($p < 0.01$) between the MLD and the import of nitrate into the surface layer. Similar evolutions for the transports of phosphate and silicate have been obtained, as expected (not shown). A strong positive correlation between the convection intensity and the surface nutrient enrichment was also obtained by *Herrmann et al*. [2013].

Table 2 gathers the annual amounts of the nutrients injected in the 0–100 m upper layer during the winter period of year 2003–2004 to year 2007–2008. We have found that the winter nutrient vertical transport presents a relative large range of variations during the study period. It varies from -136.10^3 tN (net downward export in 2006–2007) to 1222.10^3 tN (net import into the surface layer in 2004–2005) (mean value: 490 ± 500.10^3 tN) for nitrate, from -29.10^3 tP to 117.10^3 tP (mean value: 42 ± 54.10^3 tP) for phosphate, and from -208.10^3 tSi to 1840.10^3 tSi (mean value: 650 ± 749.10^3 tSi) for silicate. As a matter of comparison, *Pujo-Pay and Conan* [2003] estimated, based on in situ observations over the period 1992–1995, a nitrate enrichment of the surface layer between December and April of 260–390 mmol m^{-2} yr^{-1}, which would represent 535–802 10^3 tN at the scale of the NWMOS. Moreover, *Severin et al*. [2014] estimated surface layer replenishments during two convection events taking place in February and March 2011, using Cascade cruise observations. They obtained amounts of 193 10^3 tN of nitrate, 20 10^3 tP of phosphate, and 336 10^3 tSi of silicate, for both events. Therefore our estimates are in the same range as the previous ones based on in situ observations.

5.3. Budget of Organic Carbon

The stock of organic carbon modeled in the NWMOS (not shown) remains stable over the 5 years under study, when considering the surface layer (0–100 m, mean loss of 2% yr^{-1}) and the whole water column (mean loss of 0.3% yr^{-1}). The interannual variability of the standing stock has been estimated. A gain of organic carbon has been found for "cold" winter years and a loss of organic carbon has been highlighted in 2006–2007 and 2007–2008 when vertical mixing remains shallow; these findings are in agreement with modeling results of *Auger et al*. [2014]. Thus, the slight decreases of the stock of organic carbon over the 5 year study period are attributed to the succession of two mild winters encountered in 2006–2007 and 2007–2008. Nevertheless, the quasi-equilibrium of the standing stock enables us to estimate and to analyze a budget of organic carbon over the study period.

5.3.1. Primary Production

The modeled Gross Primary Production (GPP) presents a strong seasonal signal (Figure 9c). It is generally characterized by an increase between January and April, with a peak value in March/April; it is quite constant from June to August, with values included in the range 1–1.2 gC m^{-2} d^{-1}. It decreases then from September to the end of December despite the increase in surface chlorophyll mentioned in section 4.1. As suggested by *Lavigne* [2013] based on in situ observations this increase is the result of the entrainment of the deep chlorophyll maximum at the surface by wind-induced mixing. The evolution of the GPP for the five investigated years is highly variable during the first semester but very regular from July to January. The interannual variability of the GPP evolution during the first semester is clearly linked to the one of the atmospheric and hydrodynamic conditions, as the intense vertical mixing events cause an interruption, or at least a reduction, of the GPP winter increase, as found by *Bernardello et al*. [2012] using 3-D modeling. We have estimated the date of the onset of the annual bloom as the first day (after 1 January) when primary production (instead of surface chlorophyll as in *Siegel et al*. [2002]) is 5% greater than the annual median value. As expected, the bloom starts earlier in weakly mixing winters (28 February 2007 and 3 March 2008) than in cold winters (15 March 2005 and 16 March

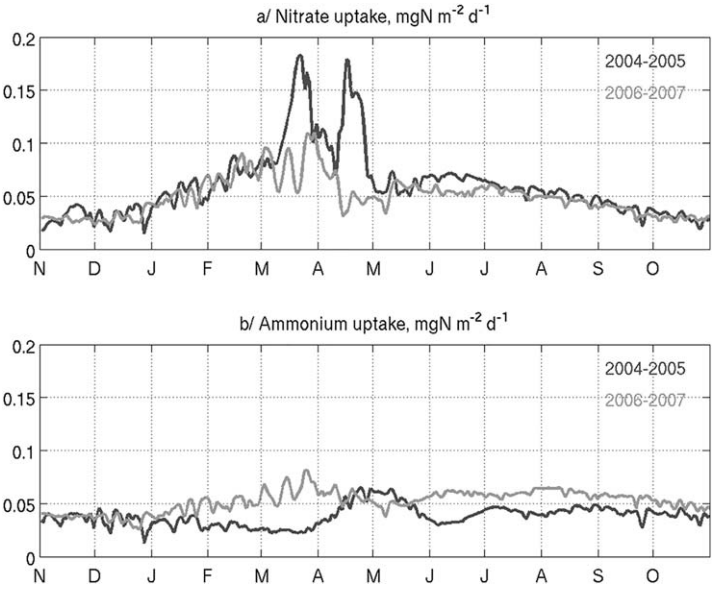

Figure 10. Seasonal time series of (a) nitrate and (b) ammonium uptakes (mgN m^{-2} d^{-1}) averaged over the NWMOS box for year 2004–2005 (dark grey) and year 2006–2007 (light grey).

2006) when deep convection takes place until mid-March. The onset of the bloom thus varies in our modeling, in a 2-week interval over the period 2004–2008, characterized by highly variable winter mixing intensities. Moreover, one can notice that the annual peak value is also correlated with the intensity of winter heat losses (Figure 3a). The modeled GPP maximum is 1.5 gC m^{-2} d^{-1} and is reached on 28 April in 2005, whereas it is smaller than 1.2 gC m^{-2} d^{-1} and is reached on 9 April in 2007, i.e., almost 3 weeks earlier than in 2005.

The range of the modeled GPP, its seasonal variations as well as the interannual variations of the maxima, are in good agreement with the results of *Bosc et al.* [2004] using SeaWiFS observations on the period 1997–2001, and the results of *Marty and Chiavérini* [2002] using in situ monthly measurements at DYFAMED station for the period 1993–1997 (the model results at the DYFAMED site—not shown—are quite similar to those averaged on the whole NWMOS region). They found a range of variations, respectively, of 0.2–1.3 gC m^{-2} d^{-1} and 0.1–1.8 gC m^{-2} d^{-1} and a peak value in March/April. However, the GPP could be overestimated in the model from August to November. Indeed, the modeled GPP varies on that period between 1 gC m^{-2} d^{-1} and 0.5 gC m^{-2} d^{-1}, while it is smaller than 0.5 gC m^{-2} d^{-1} in both observational studies.

Model results show that the contribution of nanophytoplankton to the total primary production generally dominates from January to September (Figure 9c). Microphytoplankton dominates over picophytoplankton when nutrients concentration is high in the surface layer, from January to March. The largest contribution of picophytoplankton is encountered during the stratified period, between July and November. This seasonal contribution of the three size classes of phytoplankton is in good agreement with the results of *Uitz et al.* [2012] deduced from satellite images.

Table 2 gives the values of annual and seasonal (winter and spring) primary productions during the five studied years. We found that the annual GPP and NPP (Net Primary Production) present a low interannual variability, with a mean value of 283 ± 5 gC m^{-2} y^{-1} and 150 ± 3 gC m^{-2} y^{-1}, respectively. Globally, on the 5 year period, microphytoplankton contributes to 23%, nanophytoplankton to 48%, and picophytoplankton to 28% of the total GPP. The modeled annual values fall in the range or are higher than previous estimates on the area. *Marty and Chiavérini* [2002] estimated a highly variable primary production ranging from 86 to 232 gC m^{-2} y^{-1}, but these results could be biased by the monthly frequency of the measurements. On the contrary, *Bosc et al.* [2004] estimates presented a weak interannual variation (standard deviation lower than 12%) and were in the range 180–213 gC m^{-2} y^{-1} in the Gulf of Lions and the Ligurian Sea. As found by *Auger et al.* [2014], the model results suggest that the annual GPP is not correlated with the intensity of winter mixing. However, one can notice, as shown by these authors and by *Herrmann et al.* [2013], that the winter GPP is anticorrelated with winter mixing: it is minimal in 2004–2005 when convection is very intense and maximum in 2006–2007 and 2007–2008 when winter mixing is shallow (Table 2). Conversely, the spring GPP appears to be in coherence with winter mixing: it was maximal during years of intense winter mixing characterized by strong import of nutrients into the surface layer. The winter and spring GPP interannual standard deviations (respectively 29 and 35 gC m^{-2} y^{-1}) are higher than the annual GPP one (5 gC m^{-2} y^{-1}). These results confirm that the intensity of the spring and winter GPP is tightly linked since they complement each other.

The modeled uptakes of nitrate and ammonium by phytoplankton are shown for the coldest winter year 2004–2005 and the mildest winter year 2006–2007 on Figure 10. First, both nitrate and ammonium uptakes

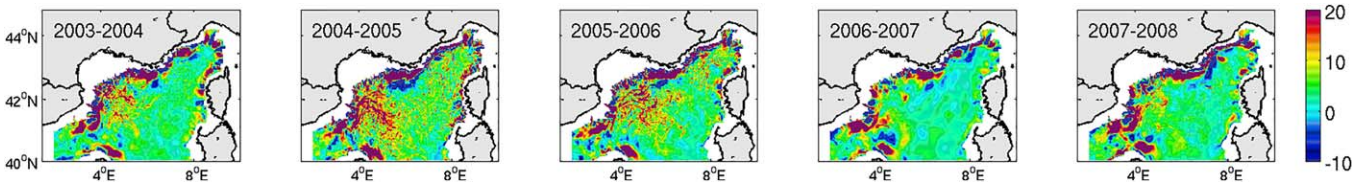

Figure 11. Annual mean export flux of organic carbon (mmolC m^{-2} d^{-1}) modeled at 100 m depth from year 2003–2004 to year 2007–2008 (positive values for downward fluxes).

show strong differences in time evolution between 2004–2005 and 2006–2007. In year 2004–2005, when the water column restratifies, a first explosive increase of nitrate uptake occurs in mid-March, and is followed by a maximum of ammonium uptake in late April/early-May. A second peak of nitrate uptake occurs after a last vertical mixing event in mid-April. In contrast, year 2006–2007 is characterized by a succession of small and short nitrate and ammonium uptake events. Second, it is interesting to notice that the nitrate uptake is similarly increasing in both early winters (January and February), no matter the amount of upwelled nutrients (Figure 9b). Finally, one can notice that in March, the ammonium uptake remains weak in 2004–2005 whereas it appears to be increasing and variable in 2006–2007. Consequently, the excess of GPP during winter 2006–2007, with regard to the GPP during winter 2004–2005 (Table 2, Figure 9c), is sustained by the uptake of ammonium which corresponds to regenerated production.

5.3.2. Export of Particulate and Dissolved Organic Carbon Toward the Bottom

5.3.2.1. Export in Subsurface

Figure 9d displays the evolution of particulate and dissolved organic carbon export toward the bottom at 100 m depth, from November 2003 to November 2008, averaged on the NWMOS. The export flux of POC ranges from 15 to 420 mgC m^{-2} d^{-1}, whereas the export of DOC ranges from 0 to 175 mgC m^{-2} d^{-1}. They fluctuate along the year and show higher values during the first semester, between January and June. Their evolutions mainly follow the one of MLD (Figure 3b) with a peak value in March. Their respective correlations with the MLD are found to be 0.76 for POC and 0.69 for DOC ($p < 0.01$). In the other hand, the export at 100 m seems not to be directly related to the OC content in the upper layer (0–100m). Indeed, the concentration of OC decreases in the surface layer during convection episodes due to the winter wind-induced dilution, when export increases. In spring, when the OC content increases during the phytoplankton bloom, the water column is stratified and the export toward the bottom is limited. Finally, in summer and early fall, both surface OC content and export slowly decrease. Significant anticorrelations are found between the export flux and the surface layer content (-0.46 for total OC, -0.14 for POC and -0.43 for DOC). These results are in fair agreement with the ones of *Miquel et al.* [2011] who reported, from in situ measurements, a better connection of the downward fluxes to the MLD than to the phytoplankton biomass. However, as shown by *Bernardello et al.* [2012], we have found that the timing of the wind-induced mixing compared to the one of phytoplankton growth has an importance in the amount of export. For instance, in 2006, after a period of deep vertical mixing in January, the water column restratifies and the phytoplankton growth starts. This first increase of phytoplankton biomass stops when a secondary intense mixing event occurs in March, provoking the maximum peak export over the 5 year studied period. The export flux appears then largely influenced both by the intensity of the mixing events and by their timing compared to the one of phytoplankton growths.

The interannual variability of annual export is clearly related to the meteorological and hydrodynamic forcing: the higher the winter heat loss, the higher the annual flux of OC export. The annual exports of POC and DOC in the NWMOS vary, respectively, from 18.6 to 36.0 gC m^{-2} y^{-1} and 11.3 to 20.1 gC m^{-2} y^{-1} over the study period (Table 2). It is noteworthy that the annual export of POC and DOC at 100 m is not negligible, but half as much, in 2006–2007 and 2007–2008, compared to the other years although winter mixing is very weak.

The annual export of POC at 100 m depth represents from 6 (in 2006–2007) to 13% (in 2004–2005) of the annual GPP. It is mainly composed of detritus material. This latter represents 72% (59% small particles, 13% large particles) of the total exported POC. Phytoplankton contributes to 10%, zooplankton to 7%, and bacteria to 11%.

Figure 9e details the contributions of sedimentation, vertical advection, and turbulent mixing to the export of POC. Sedimentation, as a quite steady component of the total export, ranges between ~6 and ~30 mgC

m^{-2} d^{-1}. It shows a seasonal cycle with a maximum in April/May, when the concentration of POC in the 0–100 m surface layer is the largest. It presents a low interannual variability (standard deviation lower than 12%) and represents from 20 (in 2004–2005) to 34% (in 2006-2007) of the total export (Table 2). The export parts due to advection and turbulent mixing clearly present greater fluctuations and their evolutions are correlated with the one of the MLD. Export by advection processes is the main component of export all over the year. Its contribution varies from 65 to 69%. Finally, export by turbulent mixing occurs only during convection events. Its weaker contribution ranges from 1 (in 2006–2007) to 13% (in 2004–2005) of the total export.

The spatial distribution of the organic carbon export at 100 m depth is displayed in Figure 11. For all years, the export is strong along the slope especially at the entrance of the Gulf of Lions, in the Catalan Canyons, and North of Minorca Island, due to advection processes along the thermohaline circulation. High values of export are also visible in the convection area, due to both advection and turbulent mixing that presents, as expected, a similar distribution (not shown) to the MLD one (Figure 4). The spatial structures of export are clearly finer during the highly convective years in 2003–2004, 2004–2005, and 2005–2006 when additional sub-mesoscale structures specifically develop.

The seasonal variability of the modeled subsurface POC export for the NWMOS is in good agreement with the general trend described by *Miquel et al*. [2011] and *Stabholz et al*. [2013] deduced from sediment trap observations, respectively, at the DYFAMED and the LION sites. They observed (1) low export fluxes during the stratification period, from June to November, (2) rapid downward transfer of particulate and dissolved matter during the vertical convection in winter, and (3) vertical export of dissolved and particulate matter controlled by phytoplankton blooms in spring. When it comes to interannual variability, it appears not relevant to compare the export obtained from model results and observations: indeed, strong currents (speed $>$ 10 cm s^{-1}) are likely to bias the trapping of particles [*Buesseler et al*., 2007]. In particular, sediment trap data in 2005 and 2006 at the DYFAMED site were not considered as reliable due to the occurrence of strong currents during the deep convection episodes [*Martín and Miquel*, 2010; *Miquel et al*., 2011].

From a quantitative point of view, *Miquel et al*. [2011] reported export fluxes at 200 m depth ranging from 0.3 to 59.9 mgC m^{-2} d^{-1}, and a mean value of 7 mgC m^{-2} d^{-1}, at the DYFAMED station. At the same site, for the sedimentation part of the POC export, we found values ranging from 2.9 to 36 mgC m^{-2} d^{-1} with a mean value of 12 mgC m^{-2} d^{-1} (std: 6 mgC m^{-2} d^{-1}). These results are in the same order of magnitude than the one deduced from sediment trap measurements. Higher values in the model results could be explained by the large fluxes during deep convective years that could have not been caught by sediment traps. *Gogou et al*. [2014] estimated a vertical export flux at 100 m of 64 mgC m^{-2} d^{-1} for the period from September 2007 to September 2008 at the LION site, based on an extrapolation at 100 m of a mean value of sediment trap flux measurements at 1200 m depth, using *Martin et al*. [1987] formulations. At this location and for the same period, we estimated a lower vertical export flux of 31 mgC m^{-2} d^{-1}.

Regarding DOC export, *Avril* [2002], using in situ monthly measurements, obtained an annual DOC flux of 12 gC m^{-2} y^{-1} (with $\pm$ 50% interannual variation) at 100 m depth at the DYFAMED station. As previously mentioned, those measurements were performed on the period 1991–1994, when winter mixing was rather weak [*Auger et al*., 2014]. We found an export of DOC with a mean value of 38 gC m^{-2} y^{-1} at the 100 m interface at this site; this modeled value is likely to be too strong due to a probable overestimation of advection processes at this point [*Auger et al*., 2014]. Nevertheless, our estimate on the whole NWMOS, namely 15.2 $\pm$ 3.8 gC m^{-2} y^{-1}, is close to the estimates of *Avril* [2002].

5.3.2.2. Export at Middepth

At 1000 m depth, the POC export follows similar seasonal signal, interannual variability, and spatial patterns of the one at 100 m depth, in the model simulations (not shown). The mean annual export of POC is found to be 4.3 $\pm$ 1.6 gC m^{-2} y^{-1} (Table 2, 16% of the mean annual export flux at 100 m). It represents from 1 to 2% of the annual GPP. In addition, we found that 71% of the annual POC export is explained by sedimentation, 29% by advection, and 1% by turbulent mixing. Again, one can notice large interannual variations in these percentages. In 2004–2005 and 2005–2006, characterized by strong deep convection, export is codominated by advection processes and sedimentation while during years of low winter mixing, 2006–2007 and 2007–2008, advection processes are responsible of less than 10% of the export. Besides, the mean annual export is mainly (70%) composed of large detritus (in agreement with sediment trap measurements reported by *Miquel et al*. [1994]); small detritus, bacteria, zooplankton, and phytoplankton count for

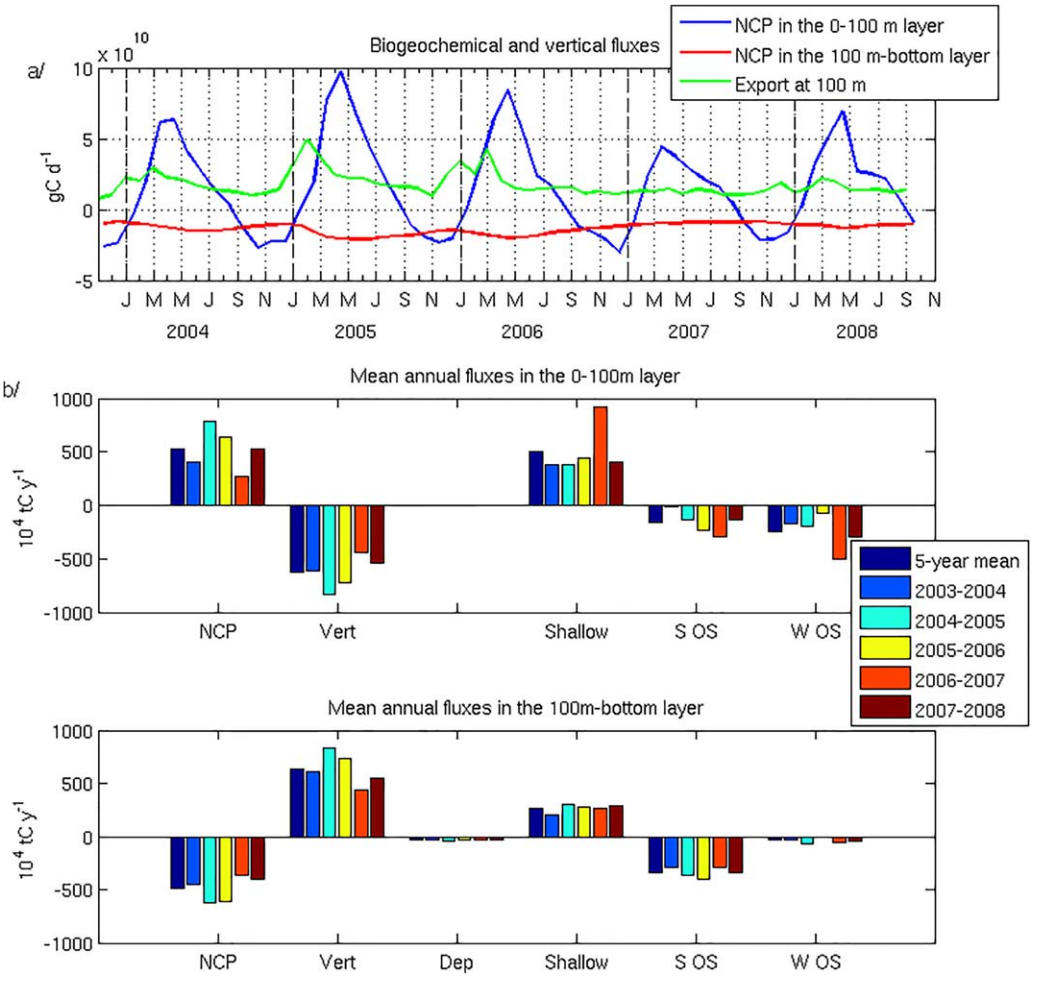

Figure 12. Budget of organic carbon (OC) in the NWMOS box: (a) time series of the monthly averaged downward OC export at 100 m depth (in green), net community production (NCP) in the surface layer (0–100m, in blue), and in the rest of the water column (100 m-bottom, in red), in gC d^{-1}; (b) 5 year mean and annual net community production (NCP), vertical transport (Vert), deposition (Dep), horizontal transports from the shallower regions (Shallow), as well as from the Southern (S OS) and Western (W OS) adjacent open seas, in the surface layer (on the top), and in the rest of the water column (below), in 10^4 tC y^{-1}. Positive values correspond to an import for the considered subbox.

respectively 15%, 8%, 6%, and 1% (not shown). The quality of the exported material changes with the intensity of deep convection. Indeed, the contribution of small detritus and living organisms increases in 2004–2005 and 2005–2006, when advection processes and sedimentation codominate the export. As a result, for instance in 2004–2005, large particles only represent 45% of the export, and the contribution of small detritus is 31%, bacteria 13%, zooplankton 8%, and phytoplankton 3%.

Stabholtz et al. [2013], *Gogou et al*. [2014]—both at the LION site—and *Miquel et al*. [2011], at the DYFAMED site, reported annual fluxes near 1000 m depth of, respectively, 2.4 gC m^{-2} y^{-1}, 1.9 gC m^{-2} y^{-1} and 1.6 gC m^{-2} y^{-1}. Our estimations of the sedimentation part of the export reach 2.8 ± 0.2 gC m^{-2} y^{-1} at the LION site, and 2.6 ± 0.2 gC m^{-2} y^{-1} at the DYFAMED site; they are thus comparable to the fluxes deduced from sediment trap measurements.

5.3.2.3. Deposition

The spatially averaged flux of POC reaching the floor of the NWMOS has been finally examined. It is characterized by a seasonal pattern with maxima in spring (late April–early May) and minima in January (not shown). Our estimate ranges from 0.2 to 1.1 mmolC m^{-2} d^{-1} and presents a mean annual value of 2.3 ± 0.2 gC m^{-2} y^{-1} (Table 2). The annual deposition flux represents 0.7% (in 2006–2007) to 0.9% (in 2003–2004, 2004–2005, and 2007–2008) of the annual GPP. The annual deposition is the largest during the intense convective year 2004–2005. The large detritus represents in average 98% of the deposition. The quality of the

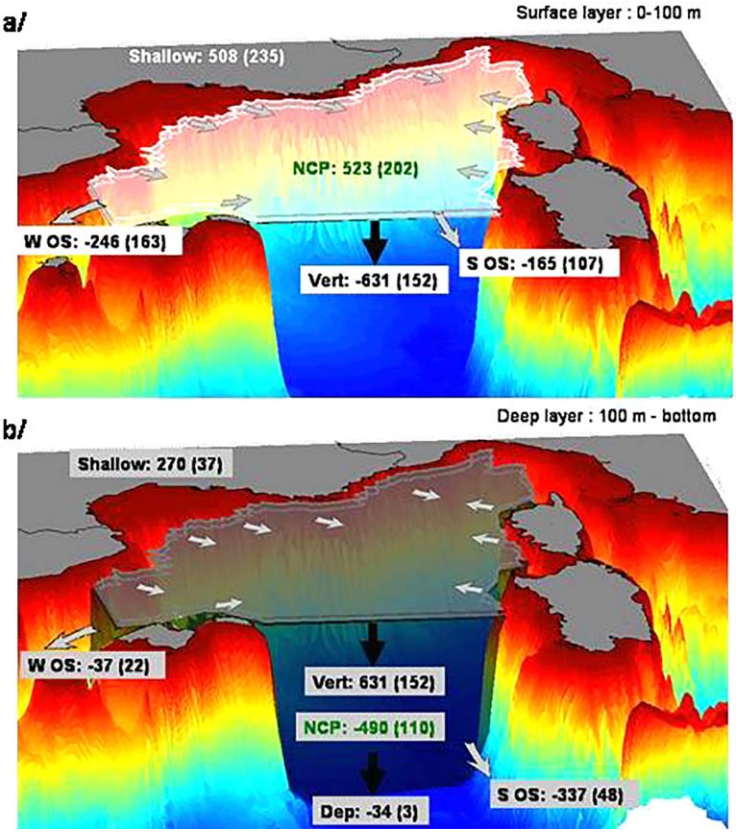

Figure 13. Five year mean and standard deviation of net community production (NCP), OC import vertical transport (Vert), OC deposition on the floor (Dep), OC lateral transports from the shallower regions (Shallow), the Southern (S OS) and Western (W OS) adjacent open seas, in the NWMOS box, (a) in the surface layer (0–100 m) and (b) in the rest of the water column (100 m-bottom), in 10^4 tC y^{-1}.

exported POC presents a low interannual variability. For instance, the part of small detritus ranges from 0.4% in 2006–2007 to 3.4% in 2004–2005.

We observe in the model simulations that most of the particles exported by sedimentation to 1000 m depth, eventually settle on the floor. Indeed, the correlation between the deposition flux and the export by sedimentation at 1000 m reaches 0.98 ($p < 0.01$). By contrast, only a limited amount of the particles entrained below 1000 m depth by advection and turbulence mixing reaches the floor: the correlations of the deposition flux with the export at 1000 m depth by advection and by turbulent mixing are found to be respectively 0 and 0.2. Note that the spatial distribution of deposition on the floor is mainly shaped by the bathymetry (not shown).

Offshore the Gulf of Lions, at the LION station, our mean annual estimates are around 2.4 ± 0.2 gC m^{-2} y^{-1} on the study period, and 2.6 gC m^{-2} y^{-1} on the period 2007–2008: these values are in agreement with the sediment traps measurements reported by *Stabholz et al.* [2013] who found 2.7 gC m^{-2} y^{-1} on the period 2008–2009, and *Gogou et al.* [2014] who estimated a deposition of 1.3 gC m^{-2} y^{-1} in year 2007–2008. It is however important to note that resuspension processes were not taken into account in our modeling studies, so that these modeled mean values might be slightly overestimated. Indeed *Martin et al.* [2010] and *Stabholz et al.* [2013] claimed that intense open ocean convection events in the NWMOS can cause strong near-bottom currents and significant remobilization of sediment.

5.3.3. Global Budget of Organic Carbon in the NWMOS

Finally, based on model accuracy, we present for the NWMOS region, an annual OC budget of the biogeochemical processes fluxes, the vertical transport, and the lateral transports to the shallower regions as well as to the adjacent Southern and Western open seas. We distinguish the surface layer (0–100 m) and the rest of the water column (100 m-bottom) in this budget calculation. First, seasonal and interannual variations of these fluxes and transports are presented. The specificity of the vigorous winters 2004–2005 and 2005–2006 is then analyzed and an annual budget is finally assessed. Figures 12 and 13 display these annual and 5 year mean budgets.

5.3.3.1. Seasonal and Interannual Variations

In the surface layer, the balance of the biogeochemical processes, corresponding to the Net Community Production (NCP), exhibits a strong seasonal signal (Figure 12a): it is positive from January to August, with a peak in March–April reaching 4.4 10^{10} gC d^{-1} in 2006–2007, and 9.7 10^{10} gC d^{-1} in 2004–2005 (monthly mean values). The minimum monthly values in October, November, and December are of the order of −2.0 10^{10} gC d^{-1}. In the rest of the water column (deeper than 100 m), the NCP is less variable than in the surface. It generally decreases from December to April when it reaches about −1.5 10^{10} gC d^{-1}. This reflects

the increase in remineralization processes when the content of OC increases during the vertical mixing events. The minimum of NCP over the whole period ($-2.\ 10^{10}$ gC d^{-1}) is reached after the deep convective winter 2004–2005 while no decrease was simulated after the mild winter 2006–2007.

The monthly-mean vertical downward transport of OC at 100 m depth also displays a clear seasonal signal (Figure 12a) as expected. Peaks are reached between January and March according to the timing of vertical mixing. Specifically, the 5-year mean vertical downward transport of POC and DOC reaches its maximum respectively at 2.1 10^{10} gC d^{-1} in March, and 0.9 10^{10} gC d^{-1} in January (data not shown).

The monthly-mean surface lateral transport of OC, from shallower regions to the NWMOS area, is globally positive during the whole year (not shown). It presents higher values in winter (between 2 10^{10} and 4 10^{10} gC d^{-1}, from November to March) than in summer (between 0.1 and 0.6 10^{10} gC d^{-1} from June to September). This evolution is rather complex to analyze considering the differences in the functioning of the various shallower adjacent regions (Corsica shelf, Ligurian Sea, Gulf of Lions, Balearic Sea) that influence this transport. If taking only into account the exchanges with the shallow regions of the Gulf of Lions and the Balearic Sea, the seasonal signal is notably different: an increase in the lateral transport takes place from December to April when it reaches a maximum of $\sim$0.7 10^{10} gC d^{-1} for both POC and DOC and after a plateau it decreases in October. This evolution is consistent with the one of primary production on these shelves. The lateral transport of OC from shallow regions in the rest of the water column is generally weak (ranging between -0.08 and 0.09 10^{10} gC d^{-1} for POC and between 0.2 and 1.3 10^{10} gC d^{-1} for DOC) with minimum values from April to June. If we considered only the transports in the Gulf of Lions and Balearic Sea regions, we obtained values which are globally smaller than 0.05 10^{10} gC d^{-1} for POC and 0.8 10^{10} gC d^{-1} for DOC, except during two periods: from March to October 2005 and from March to September 2006, that will be discussed in section 5.3.3.2 below.

The monthly-mean transport from the NWMOS to the Southern open sea follows a seasonal cycle which is similar to the one of the transport from shallow region to NWMOS in the whole water column (not shown). In the surface layer, it is maximum in November (1.2 10^{10} gC d^{-1} for POC and 2.7 10^{10} gC d^{-1} for DOC) and minimum in May (-0.5 10^{10} gC d^{-1} for POC and DOC). The monthly-mean transport from NWMOS to the Western open sea is always positive, except in October, with maxima from January to May (1.4 10^{10} gC d^{-1} in the surface layer, 0.3 10^{10} gC d^{-1} in the rest of the water column).

5.3.3.2. Vigorous Winters 2004–2005 and 2005–2006

During the convection events of 2004–2005 and 2005–2006, we have estimated a vertical OC export of, respectively, 4.1 10^{10} gC d^{-1} (POC: 2.7 10^{10} gC d^{-1} and DOC: 1.4 10^{10} gC d^{-1}) and 3.2 10^{10} gC d^{-1} (POC: 2.0 10^{10} gC d^{-1} and DOC: 1.2 10^{10} gC d^{-1}). This corresponds to an amount of exported OC reaching 3.1 10^{6} tC for 2004–2005 events and 3.3 10^{6} tC for 2005–2006 events. Our estimation of DOC export is comparable but lower than the estimate performed by *Santinelli et al*. [2010] that ranged from 2.5 to 9.9 10^{10} gC d^{-1} for the 2004–2005 events. For their estimation, these authors used the mean production rate of dense water (2.4 Sv) deduced by *Schroeder et al*. [2008] from observations, multiplied by a constant value of surface (0–50m) winter DOC concentrations (10–40 mmol m^{-3}). However, as mentioned before, recent observations collected during DEWEX1 campaign show homogeneous profiles of DOC in the MEDOC area during winter mixing (M. Pujo-Pay, personal communication). In the model, such homogenizations of DOC profiles, and hence decreases of surface DOC concentration, are represented during intense vertical mixing. Thus, the spatiotemporal variation of the modeled surface DOC concentration could explain that we obtained a lower estimation than the one derived from observations by *Santinelli et al*. [2010].

Winters 2004–2005 and 2005–2006 were also characterized by intense and deep dense shelf water cascading along the Gulf of Lions and Catalan slopes [*Lopez-Jurado et al*., 2005; *Canals et al*., 2006; *Ulses et al*., 2008]. *Santinelli et al*. [2010] reported high DOC concentrations near the bottom in the Western part of the Balearic Front in May 2005 that may be explained by this physical process. We have estimated the lateral transports of OC, associated to these dense shelf water (DSW) cascading events, from the Gulf of Lions and Balearic Sea shallow areas to the NWMOS. These estimations reach 1.5 10^{10} gC d^{-1} for 2004–2005 events and 0.7 10^{10} gC d^{-1} for 2005–2006 events. This corresponds to amounts of exported OC reaching 3.2 10^{6} tC (0.7 10^{6} tC POC and 2.5 10^{6} tC for DOC) for 2004–2005 event and 1.6 10^{6} tC (0.3 10^{6} tC for POC and 1.3 10^{6} tC for DOC) for 2005–2006 event. Our results are close to the estimates performed for the 2004–2005 cascading event by *Canals et al*. [2006] of 1.5 10^{10} gC d^{-1}, based on sediment traps, and by *Ulses et al*. [2008] that ranged between 1.4 and 2.9 10^{6} tC, based on 3-D hydrodynamic modeling.

It is also noteworthy that we have obtained an estimate of the lateral OC transport due to DSW cascading very close to the estimate of vertical OC export during the open sea convection event of the same year 2004–2005 mentioned before (3.2 10^6 tC versus 3.1 10^6 tC), although the amount of exported dense water associated to cascading events is much lower than the one induced by open-sea convection ($\sim$8 10^{13} m^3 of DW formed during open-sea convection versus $\sim 10^{12}$ m^3 of DW exported by cascading).

5.3.3.3. Annual Budget

At the annual scale, the NCP appears to be positive in the surface layer of the NWMOS (5 year mean: 523 ± 202 10^4 tC y^{-1}, Figures 12b and 13a). Besides, the NWMOS appears as a sink for organic carbon originated from shallow areas: the 5 year mean lateral transports from the margin are 508 ± 235 10^4 tC y^{-1} in the surface layer. These inputs in the surface layer are exported toward the bottom (5 year mean: 631 ± 152 10^4 tC y^{-1}) and toward the surface layers of the Southern (5 year mean: 165 ± 107 tC y^{-1}) and Western (5 year mean: 246 ± 163 10^4 tC y^{-1}) open seas. It is noteworthy that the vertical downward export of OC is higher than the surface NCP (5 year mean: 121% of the surface NCP). In the rest of the water column (100 m-bottom, Figure 13b), the OC imported by vertical transports from the upper layer and by lateral transports from the shallow areas (5 year mean: 270 ± 37 tC y^{-1}), is either locally remineralized in the water column (5 year mean: 490 ± 110 tC y^{-1}), or exported mainly to the Southern open sea (5 year mean: 337 ± 48 tC y^{-1}).

Annual surface layer NCP and downward export increase with the intensity of the mean winter heat loss (Figure 12b). An inverse trend is visible for NCP in the rest of the water column. This is explained by the fact that during years characterized by vigorous winters, an important part of heterotroph processes is shifted from the surface to the deep waters, as higher amounts of OC are exported toward the bottom during mixing events. If open sea convection tends to reduce in frequency and intensity in the future because of an increasing stratification and the weakening of the thermohaline circulation [*Somot et al*., 2006; *Herrmann et al*., 2008] the NCP in the surface layer and the downward export of OC may then decrease. Regarding the lateral transports, no clear connection with atmospheric forcings or with hydrodynamic conditions is evidenced.

5.3.4. Sensitivity Studies

The fluxes and transport budget terms discussed up to now (reference results) were calculated by considering an analysis domain including the deep convection and bloom areas, and based on the definitions from *D'Ortenzio and Ribera d'Alcala* [2009], *Bernardello et al*. [2012], and *Auger et al*. [2014] (2°E < longitude < 9.5°N; 40°N < latitude < 45°N; bathymetry > 1500 m, see section 2.1.3). Two additional simulations have been performed to assess the sensitivity of model results to the choice of the analysis domain boundaries. In a first test, the area has been extended toward the coast by modifying the boundary isobath from 1500 to 1000 m. In a second test, the area has been inversely reduced with a boundary isobath set to 1700 m.

Table 3. Results of the Sensitivity Study, in Terms of Ratios Between the 5 Year Average of the Annual Fluxes Obtained in Sensitivity Tests and the Ones Corresponding to the Reference Simulation

		Isobath 1000 m	Isobath 1700 m
GPP		1.009	0.996
NPP		1.001	0.999
POC export	at 100 m	1.054	0.947
	at 1000 m	1.068	0.956
DOC export at 100 m		0.969	0.951
Deposition		1.115	0.941
Nitrate transport at 100 m		0.984	0.934
Phosphate transport at 100 m		1.207	0.909
Silicate transport at 100 m		1.053	0.923
NCP	0–100 m	1.046	0.964
	100 m-bottom	1.124	0.934
OC lateral fluxes at the boundary of the NWMOS			
Boundary with shallow regions	0–100 m	0.778	1.066
	100 m-bottom	1.145	1.013
Boundary with the Western open sea	0–100 m	0.985	1.056
	100 m-bottom	0.965	0.865
Boundary with the Southern open sea	0–100 m	0.399	1.197
	100 m-bottom	0.972	1.033

It is noteworthy that the time evolution and the interannual variability of the annual fluxes (not shown) are not significantly modified in both tests. Table 3 provides the ratios between the mean annual fluxes obtained with boundary changes, and the ones of the reference simulation. The modification of the analysis domain boundaries has a negligible impact on the mean annual primary productions (changes less than 1%). The OC exports (at 100 m and 1000 m depth) present a change of less than 7%. The deposition flux in the area delimited by the 1700 m isobath is reduced by 6%; it is reinforced by 11% when the area is delimited by the 1000 m isobath. The upward transports of nutrients change by 8–9% for the reduced domain (isobath 1700 m) and by 5–21% for the extended domain. This could be explained by the strong gradient of nutrients at 100 m and the strong vertical dynamics along the slope. The NCP is increased in the whole water column in the extended domain and inversely in the reduced domain. Finally, important impacts on certain lateral transports (*i.e.,* change of 22% in the transport towards the shallower regions and up to 60% in the transport toward the Southern open sea, both in the surface layer) are found, probably due to strong mesoscale dynamics in the slope currents.

6. Conclusion and Perspectives

A recalibrated version of the 3-D physical-biogeochemical coupled model described by *Auger et al*. [2011] has been used in order to appraise the interannual variability of transport and biogeochemical fluxes in the NWMOS over the period 2004–2008. This period is marked by highly contrasted winter atmospheric and hydrodynamic conditions. The confrontation of model results with in situ and satellite observations on that period shows the capabilities of the model to correctly capture the timing, the intensity, and the spatial extent of the open-sea convection and spring bloom events.

The results confirm that the amount of nutrients injected in the productive zone is highly dependent on the intensity of winter mixing. A strong import of nutrients (1222.10^3 tN of nitrate, 117.10^3 tP of phosphate, and 1840.10^3 tSi of silicate) to the upper layer has been estimated for the 2004–2005 severe winter. On the contrary, the annual primary production does not seem to be sensitive to hydrodynamic variability. A compensation effect between winter and spring primary productions explains this result. During severe winters, the phytoplankton growth is inhibited during intense mixing events followed by spectacular new and then regenerated productions. In contrast, during mild winters, the growth of phytoplankton starts earlier and is described by a succession of moderate new and regenerated productions.

The exports of organic carbon at 100 m and 1000 m depths are found highly affected by deep convection intensity. For instance, during the year 2004–2005, marked by an extremely cold winter, the annual organic matter export at 100 m depth is twice as high than the one estimated during the mild winter year 2006–2007. The seasonal signal of the organic carbon export is marked by maxima during the events of winter mixing during which organic carbon is mostly exported by advection and turbulent mixing processes. Besides, the maximum daily export over the 5 year period is obtained in winter 2005–2006, during a violent mixing episode following a calm period favorable to phytoplankton growth.

The estimates of the biogeochemical and transport fluxes suggest that the NWMOS is an autotrophic area, since net community production is positive in the whole water column. During years of intense deep convection, an increasing part of heterotroph processes takes place in the aphotic zone, due to higher downward organic matter export fluxes. The NWMOS globally acts as a sink for organic carbon originated from shallow region, and a source of organic carbon for the adjacent open-seas, in particular for the Algerian subbasin.

Although the model gives some realistic spatial and temporal patterns, comparisons with observations highlight possible defaults. Globally, the biogeochemical module of the model presents obviously weaker performance than the physical module. First, it has been shown that the modeled surface chlorophyll concentration could be overestimated in winter. Moreover the differences between the model biogeochemical fields and the satellite observations have been found to be greater in the regions of strong submesoscale activity, on the slope and in the convection areas (MEDOC area and Ligurian Sea). This could induce an overestimation of the export which has shown to be particularly strong during winter in these regions. The new high frequency and high resolution in situ observations (in particular bio Argo floats data) that have been deployed since 2011 in that area, could be very useful to better constrain the model and hence refine the present budget. Moreover, new improvements of the model should be realized for further studies. The

impact of resuspension processes might be assessed, since *Stabholz et al*. [2013], by comparing the fluxes at middepth and near the bottom, evidenced the influence of these processes during deep open-sea convection. Besides, two surveys (DEWEX1 and DEWEX2) were carried out in February and April 2013 in the NWMOS where an unprecedented set of data concerning the carbonate system was collected. This will be a very favorable context to add in our model a dedicated module describing this system [*Soetaert et al*., 2007], in order to assess the influence of atmospheric and hydrodynamic processes on the uptake of CO_2 in this open-sea area.

Appendix A: State Variables and Model Parameters

Table A1 gathers the state variables and Table A2 the model parameters. The model equations are given in Auger et al. [2011]. Differences in parameter values relative to this article are indicated in Table A.2.

Table A1. List of State Variables

State Variables	Description	Unit
Nut_1 (NO_3), Nut_2 (NH_4), Nut_3 (PO_4), Nut_4 (SiO_4)	Nitrate, Ammonium, Phosphate, Silicate	mmol m^{-3}
$XPhy_1$, $XPhy_2$, $XPhy_3$	Pico, nano, microphytoplankton in X, X = C (carbon), N (nitrogen), P (phosphorus) or Si (silica)	mmolX m^{-3}
$ChlPhy_1$, $ChlPhy_2$, $ChlPhy_3$	Pico, nano, microphytoplankton in chlorophyll	mgChl m^{-3}
$CZoo_1$, $CZoo_2$, $CZoo_3$	Nano, micro, and mesozooplankton	mmolC m^{-3}
CBac	Bacteria	mmolC m^{-3}
DOX	Dissolved organic X, X = carbon, nitrogen, and phosphorus	mmolX m^{-3}
$XDet_Y$	Heavy (Y = H) and light (Y = L) particulate organic X, X = carbon, nitrogen, phosphorus, silica, and chlorophyll	mmolX m^{-3}

Table A2. List of Parameters of the Biogeochemical Model and References[a]

Symbol Phytoplankton	Description	Unit	Value			Reference
			Phy_1	Phy_2	Phy_3	
φ_{max,Phy_i}	Maximum quantum yield	mmolC J^{-1}	**1.6 10^{-4}**	**1.9 10^{-4}**	2.6 10^{-4}	1,2,c
a_{Chl,Phy_i}	Chl-specific absorption coefficient	m^2 $mgChl^{-1}$	0.032	0.016	0.013	2,c
τ_{Phy_i}	Renewal time of photosystems	days	2.3 10^{-8}	3.5 10^{-8}	4.7 10^{-8}	3,c
σ_{Phy_i}	Cross section of photosystems	m^2 J^{-1}	18	12	9	4,5,c
k_d	Dimensionless photoinhibition rate		2.6 10^{-8}	2.6 10^{-8}	2.6 10^{-8}	6
k_{rep}	Rate of repair of photoinhibition damaged PSII	days	2.3 10^{-9}	2.3 10^{-9}	2.3 10^{-9}	6
$(N/C)_{min,Phy_i}$	Minimal internal N/C quota	molN $molC^{-1}$	0.05	0.05	0.05	7,8,9
$(N/C)_{max,Phy_i}$	Maximal internal N/C quota	molN $molC^{-1}$	**0.2**	**0.2**	**0.2**	7,8,9
$(P/C)_{min,Phy_i}$	Minimal internal P/C quota	molP $molC^{-1}$	0.004	0.002	0.002	8,10,11
$(P/C)_{max,Phy_i}$	Maximal internal P/C quota	molP $molC^{-1}$	**0.019**	**0.019**	**0.019**	8,10,11
$(Si/C)_{min,Phy_i}$	Minimal internal Si/C quota	molSi $molC^{-1}$			0.05	9,11
$(Si/C)_{max,Phy_i}$	Maximal internal Si/C quota	molSi $molC^{-1}$			**0.19**	9,11
$(Chl/N)_{max,Phy_i}$	Maximal internal Chl/N quota	mgChl $molN^{-1}$	**2.3**	**2.3**	**2.3**	12,13,c
Q_{Phy}^{10}	Temperature coefficient		2.0	2.0	2.0	14
T_{Phy}^{REF}	Reference temperature	°C	15	15	15	15, c
k_{resp,Phy_i}	Respiration cost for growth		0.3	0.25	0.2	13,14,16,c
$\beta_{Phy_i,N}$	Nitrogen parameter for growth rate limitation	molN $molC^{-1}$		0.0072	0.002	c
$\beta_{Phy_i,P}$	Phosphorus parameter for growth rate limitation	molP $molC^{-1}$		0.0002	0.0005	c
$\beta_{Phy_i,Si}$	Silica parameter for growth rate limitation	molSi $molC^{-1}$			0.004	c
k_{Si}	Nitrogen parameter for growth rate limitation by silica	molN $molC^{-1}$			0.1	c
k_{Phy_i,NO_3}	Half saturation constant for NO_3	mmolN m^{-3}	0.5	0.7	1	11,15,17,18, c
k_{Phy_i,NH_4}	Half saturation constant for NH_4	mmolN m^{-3}	0.1	0.3	0.7	15,17,18,c
k_{inhib}	Inhibition coefficient by NH_4	mmolN m^{-3}	0.578	0.578		17
Inhib	Inhibition parameter by NH_4		0.82	0.82		17
k_{Phy_i,PO_4}	Half-saturation constant for PO_4	mmolP m^{-3}	**0.005**	**0.015**	**0.05**	11,18,19,c
k_{Phy_i,SiO_4}	Half-saturation constant for SiO_4	mmolSi m^{-3}			1.2	11,c

Table A2. (continued)

Symbol	Description	Unit	Value			Reference
Phytoplankton			Phy_1	Phy_2	Phy_3	
r_{Phy_i,NO_3}	Respiration cost for NO_3 uptake	molC $molN^{-1}$	0.397	0.397	0.397	16
r_{Phy_i,NH_4}	Respiration cost for NH_4 uptake	molC $molN^{-1}$	0.198	0.198	0.198	16
r_{Phy_i,PO_4}	Respiration cost for PO_4 uptake	molC $molP^{-1}$	0.155	0.155	0.155	16
r_{Phy_i,SiO_4}	Respiration cost for SiO_4 uptake	molC $molSi^{-1}$			0.140	16
r_{mort,PO_4}	Natural mortality rate	d^{-1}	**0.19**	0.13	0.10	7,20,c
w_{s,Phy_i}	Sinking rate	m d^{-1}			0.7	7,15,c
Zooplankton			Zoo_1	Zoo_2	Zoo_3	
g_{Zoo_i}	Maximum grazing rate	d^{-1}	3.89	**2.59**	**1.30**	7,21,22,c
k_{g,Zoo_i}	Half-saturation constant	mmolC m^{-3}	5	8.5	20	23,c
Ψ_{Zoo_i}	Messy feeding fraction		0.23	0.23	0.23	7,24
β_{Zoo_i}	Assimilation efficiency		0.6	0.6	0.6	7,24
k_{c,Zoo_i}	Net growth efficiency		0.8	0.8	0.8	7,24
$(N/C)_{Zoo_i}$	Internal N/C quota	molN $molC^{-1}$	0.18	0.18	0.18	7,10,25
$(P/C)_{Zoo_i}$	Internal P/C quota	molP $molC^{-1}$	0.013	0.013	0.013	10,25,c
τ_{mort,Zoo_i}	Natural mortality rate	d^{-1}	**0.22**	**0.17**		20,c
τ_{pred}	Predation mortality rate	m^3 (mmolC $d)^{-1}$			0.061	20,c
$fr_{Det_L}^{Eges_{Si}}$	Ratio light/heavy Si detritus in residues of egestion			0.8	0.8	c
$fr_{Det_L}^{MortZoo_i}$	Ratio light/heavy detritus in zooplankton loss term		1	1	0.95	c
Q_{Zoo}^{10}	Temperature coefficient		2.0	2.0	2.0	7
T_{Zoo}^{REF}	Reference temperature	°C	20	20	20	c
$prey_{i,Prey}$	Preference of Zooplankton i for Prey					

Zoo_i/Prey	Bacteria	Phy_1	Phy_2	Phy_3	Zoo_1	Zoo_2	Det_L
Zoo_1	0.35	0.65	0	0	0	0	0
Zoo_2	0.08	0.06	**0.25**	**0.2**	**0.25**	0.12	0.04
Zoo_3	0	0	0	0.5	0	0.45	0.05

Bacteria				
μ_{Bac}	Maximum DOC uptake	d^{-1}	**0.99**	15,24,c
k_{DOC}	Half-saturation for DOC uptake	mmolC m^{-3}	25	24
ω_{Bac}	Bacteria gross growth efficiency		0.3	24,c
$(N/C)_{Bac}$	Bacteria internal N/C quota	molN $molC^{-1}$	0.232	10
$(P/C)_{Bac}$	Bacteria internal P/C quota	molP $molC^{-1}$	0.022	10,28
$k_{NH_4,Bac}$	Half-saturation for NH_4 uptake	mmolN m^{-3}	0.2	24,c
$k_{PO_4,Bac}$	Half-saturation for PO_4 uptake	mmolP m^{-3}	0.007	25,c
$k_{mort,Bac}$	Bacteria natural mortality rate	d^{-1}	0.06	20
Q_{Bac}^{10}	Temperature coefficient		2.95	10
T_{Bac}^{REF}	Reference temperature	°C	20	c

Nonliving matter				
$\tau_{rem,CDet}$	Detritus remineralization rate, C	d^{-1}	0.04	24,c
$\tau_{rem,NDet}$	Detritus remineralization rate, N	d^{-1}	0.05	24,c
$\tau_{rem,PDet}$	Detritus remineralization rate, P	d^{-1}	0.06	28,c
$\tau_{rem,ChlDet}$	Detritus remineralization rate, Chl	d^{-1}	0.1	c
$\tau_{rem,SiDet}$	Detritus remineralization rate, Si	d^{-1}	0.005	20
w_{s,Det_L}	Light detritus sinking rate	m d^{-1}	0.7	15,c
w_{s,Det_H}	Heavy detritus sinking rate	m d^{-1}	90	15,c
Q_{rem}^{10}	Temperature coefficient for remineralization		2.95	10
T_{rem}^{REF}	Reference temperature for remineralization	°C	20	c
τ_{nitrif}	Nitrification rate	d^{-1}	0.05	15,c
Q_{nitrif}^{10}	Temperature coefficient for nitrification		2.37	10
T_{nitrif}^{REF}	Reference temperature for nitrification	°C	10	c

[a]Modifications relative to *Auger et al.* [2011] are indicated in bold. C: carbon; N: nitrogen; P: phosphorus; Si: silica; NO_3: nitrate; NH_4: ammonium; PO_4: phosphate; SiO_4: silicate; Phy_1: pico-phytoplankton; Phy_2: nanophytoplankton; Phy_3: microzooplankton; Zoo_1: nano-zooplankton; Zoo_2: microzooplankton; Zoo_3: mesozooplankton; DOC: Dissolved organic carbon; (c) Calibration; (1) [*Babin et al.*, 1996]; (2) [*Claustre et al.*, 2005]; (3) [*Laney et al.*, 2005]; (4) [*Moore et al.*, 2003]; (5) [*Gorbunov et al.*, 1999]; (6) [*Oliver et al.*, 2003]; (7) [*Raick et al.*, 2005]; (8) [*Riegman et al.*, 2000]; (9) [*Geider et al.*, 1998]; (10) [*Vichi et al.*, 2007]; (11) [*Sarthou et al.*, 2005]; (12) [*van den Meersche et al.*, 2004]; (13) [*Sondergaard and Theil-Nielsen*, 1997]; (14) [*Soetaert et al.*, 2001]; (15) [*Lacroix and Grégoire*, 2002]; (16) [*Cannell and Thornley*, 2000]; (17) [*Harrison et al.*, 1996]; (18) [*Tyrrell and Taylor*, 1996]; (19) [*Timmermans et al.*, 2005]; (20) [*Fasham et al.*, 2006]; (21) [*Christaki et al.*, 2002]; (22) [*Nejstgaard et al.*, 1997]; (23) [*Hansen et al.*, 1997]; (24) [*Anderson and Pondaven*, 2003]; (25) [*Goldman et al.*, 1987]; (26) [*Liu and Dagg*, 2003]; (27) [*Thingstad et al.*, 1993]; (28) [*Thingstad*, 2005].

Acknowledgments
This study is a contribution to the MerMEX (Marine Ecosystem Response in the Mediterranean Experiment) and HyMeX (Hydrological cycle in the Mediterranean EXperiment) projects of the MISTRALS international programme. Numerical modeling was supported by the PERSEUS project funded by the European Union under FP7, Theme "Oceans of Tomorrow" OCEAN.2011-3, grant agreement 287600 and was partly funded by the French ANR (Agence Nationale de la Recherche) through the CHACCRA project (Climate and Human-induced Alterations in Carbon Cycling at the River-seA connection). The SYMPHONIE ocean model is developed by the SIROCCO group. Sources are available at http://sirocco.omp.obs-mip.fr/ocean_models/S-model/download. We thank Cyril N'Guyen and computer engineers from the Laboratoire d'Aérologie for technical support. Numerical simulations were performed using the LA cluster and HPC resources from CALMIP (grants P1325 and P1331). The DYFAMED time-series data (LOV, Villefranche-sur-Mer, doi:10.12770/271cddd7-e9af-4175-9398-3f3e272af9bb) were provided by the national program MOOSE (supported by CNRS-INSU and ALLENVI). We are grateful to David Antoine for kindly providing with Boussole project data (http://www.obs-vlfr.fr/Boussole/html/home/home.php). We also thank Samuel Somot and Florence Sevault (Météo-France/CNRM) for running and providing with NEMOMED8 outputs. We thank the BANQUE Hydro (http://www.hydro.eaufrance.fr/) and SAIH Ebro (http://www.saihebro.com/) for providing with the river discharges, Patrick Raimbault for providing with the data of concentration of nutrients and dissolved organic matter in the Rhône river (http://mistrals.sedoo.fr/?editDatsId=767&datsId=767-project_name=MERMeX) and the CMM (Météo-France) for sensors maintenance and transmission of the LION buoy data (http://data.datacite.org/10.6096/HyMeX.LionBuoy.Thermosalinograph.20100308). The sea surface temperature satellite data were downloaded from the EOWEB Geoportal of DLR (http://eoweb.dlr.de) and Aqua-MODIS satellite data on http://disc.sci.gsfc.nasa.gov/giovanni. Additional support during the writing phase for P.-A. Auger was provided by the Instituto Milenio de Oceanografía (IMO-Chile), funded by the Iniciativa Científica Milenio (ICM-Chile). Finally, we are grateful to Prof. Dr. Jack Middelburg for providing research facilities at the NIOO center.

Appendix B: River Discharges

Figure B1 presents the time evolution of the river discharges over the study period. The time evolution of the Rhone discharge presents an important interannual variation in winter. The contribution of the Rhône represents 71% of the annual total runoff.

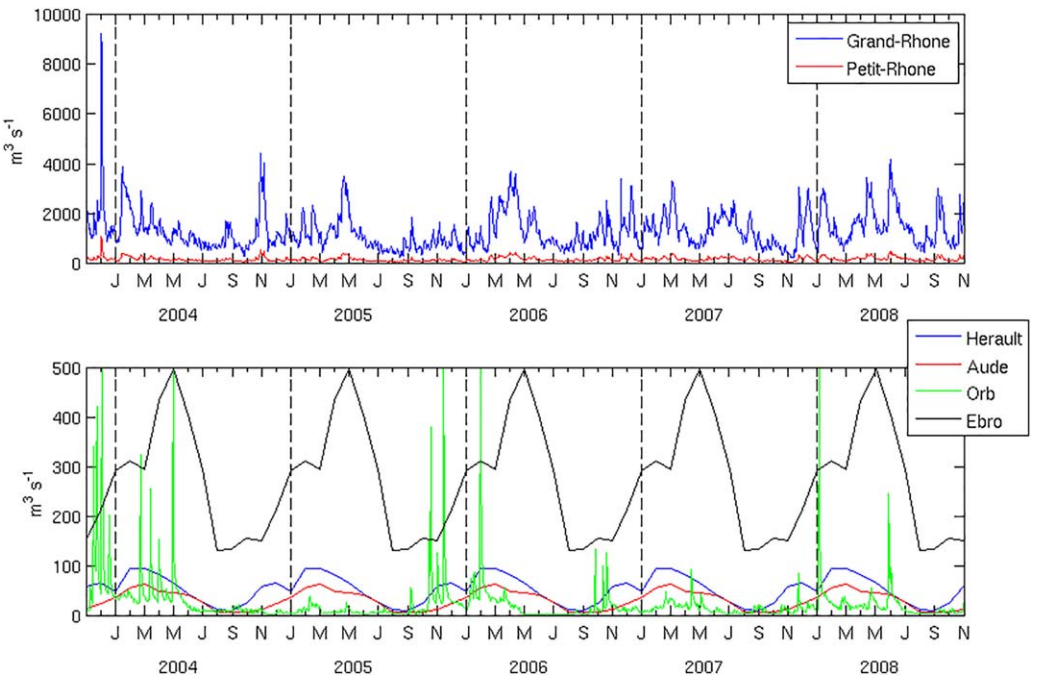

Figure B1. Discharges ($m^3\ s^{-1}$) of the Rhône, Hérault, Aude, Orb, and Ebro rivers, prescribed in the model over the study period.

References

Anderson, T. R., and P. Pondaven (2003), Non-Redfield carbon and nitrogen cycling in the Sargasso Sea: Pelagic imbalances and export flux, *Deep Sea Res., Part I*, *50*, 573–591.

Antoine, D., et al. (2006), BOUSSOLE: A joint CNRS-INSU, ESA, CNES and NASA Ocean Color Calibration And Validation Activity. *NASA Tech. Mem. 2006-214147*, 59 pp., NASA GSFC, Greenbelt, Md.

Antoine, D., F. D'Ortenzio, S. B. Hooker, G Bécu, B. Gentili, D. Tailliez, and A. J. Scott (2008), Assessment of uncertainty in the ocean reflectance determined by three satellite ocean color sensors (MERIS, SeaWiFS, and MODIS-A) at an offshore site in the Mediterranean Sea (BOUSSOLE project), *J. Geophys. Res.*, *113*, C07013, doi:10.1029/2007JC004472.

Auclair, F., P. Marsaleix, and C. Estournel (2000), Sigma coordinate pressure gradient errors: Evaluation and reduction by an inverse method, *J. Atmos. Oceanic Technol.*, *17*, 1348–1367.

Auger, P., F. Diaz, C. Ulses, C. Estournel, J. Neveux, F. Joux, M. Pujo-Pay, and J.-J. Naudin (2011), Functioning of the planktonic ecosystem on the Gulf of Lions shelf (NW Mediterranean) during spring and its impact on the carbon deposition: A field data and 3-D modeling combined approach, *Biogeosciences*, *8*(11), 3231–3261, doi:10.5194/bg-8-3231-2011.

Auger, P., C. Ulses, C. Estournel, L. Stemmann, S. Somot, and F. Diaz (2014), Interannual control of plankton communities by deep winter mixing and prey/predator interactions in the NW Mediterranean: Results from a 30-year 3D modeling study, *Prog. Oceanogr.*, *124*, 12–27, doi:10.1016/j.pocean.2014.04.004.

Avril, B. (2002), DOC dynamics in the Northwestern Mediterranean Sea (DyFaMed site), *Deep Sea Res., Part II*, *49*, 2163–2182.

Babin, M., A. Morel, H. Claustre, A. Bricaud, Z. Kolber, and P. G. Falkowski (1996), Nitrogen- and irradiance-dependent variations of the maximum quantum yield of carbon fixation in eutrophic, mesotrophic and oligotrophic marine systems, *Deep Sea Res. Part I*, *43*, 1241–1272.

Baklouti, M., V. Faure, L. Pawlowski, and A. Sciandra (2006), Investigation and sensitivity analysis of a mechanistic phytoplankton model implemented in a new modular numerical tool (Eco3M) dedicated to biogeochemical modelling, *Prog. Oceanogr.*, *71*(1), 34–58, doi:10.1016/j.pocean.2006.05.003.

Bernardello, R., J. G. Cardoso, N. Bahamon, D. Donis, I. Marinov, and A. Cruzado (2012), Factors controlling interannual variability of vertical organic matter export and phytoplankton bloom dynamics-a numerical case-study for the NW Mediterranean Sea, *Biogeosciences*, *9*(11), 4233–4245, doi:10.5194/bg-9-4233-2012.

Béthoux, J.P., X. Durrieu de Madron, F. Nyffeler, and D. Tailliez (2002), Deep water in the western Mediterranean: Peculiar 1999 and 2000 characteristics, shelf formation hypothesis, variability since 1970 and geochemical inferences, *J. Mar. Syst.*, *33–34*, 117–131.

Bosc, E., A. Bricaud, and D. Antoine (2004), Seasonal and interannual variability in algal biomass and primary production in the Mediterranean Sea, as derived from 4 years of SeaWiFS observations, *Global Biogeochem. Cycles*, *18*, GB1005, doi:10.1029/2003GB002034.

Buesseler, K.O., et al. (2007), An assessment of the use of sediment traps for estimating upper ocean particle fluxes, *J. Mar. Res.*, *65*(3), 345–416.

Canals, M., P. Puig, X. Durrieu de Madron, S. Heussner, A. Palanques, and J. Fabres (2006), Flushing submarine canyons, *Nature*, *444*, 354–357.

Cannell, M. G. R., and J. H. M. Thornley (2000), Nitrogen states in plant ecosystems: A viewpoint, *Ann. Bot. London*, *86*, 1161–1167.
Christaki, U., C. Courties, H. Karayanni, A. Giannakourou, C. Maravelias, K. A. Kormas, and P. Lebaron (2002), Dynamic characteristics of prochlorococcus and synechococcus consumption by bacterivorous Nanoflagellates, *Microb. Ecol.*, *43*, 341–352.
Claustre, H., M. Babin, D. Merien, J. Ras, L. Prieur, S. Dallot, O. Prasil, H. Dousova, and T. Moutin, T. (2005), Toward a taxon-specific parameterization of bio-optical models of primary production: A case study in the North Atlantic, *J. Geophys. Res.*, *110*, C07S12, doi:10.1029/2004JC002634.
D'Ortenzio, F., and M. Ribera d'Alcala (2009), On the trophic regimes of the Mediterranean Sea: A satellite analysis. *Biogeosciences*, *6*, 139–148.
D'Ortenzio, F., D. Iudicone, C. de Boyer Montegut, P. Testor, D. Antoine, S. Marullo, R. Santoleri, and G. Madec (2005), Seasonal variability of the mixed layer depth in the Mediterranean Sea as derived from in situ profiles, *Geophys. Res. Lett.*, *32*, L12605, doi:10.1029/2005GL022463.
Diaz, F., P. Raimbault, B. Boudjellal, N. Garcia, and T. Moutin (2001), Early spring phosphorus limitation of primary productivity in a NW Mediterranean coastal zone (Gulf of Lions), *Mar. Ecol. Prog. Ser.*, *211*, 51–62.
Dufau-Julliand, C., P. Marsaleix, A. Petrenko, and I. Dekeyser (2004), Three-dimensional modelling of the Gulf of Lion's hydrodynamics (northwestern Mediterranean) during January 1999 (MOOGLI 3 experiment) and late winter 1999: Western Mediterranean Intermediate Water's (WIW) formation and its cascading over the shelf break, *J. Geophys. Res.*, *109*, C11002, doi:10.1029/2003JC002019.
Durrieu de Madron, X., et al. (2013), Interaction of dense shelf water cascading and open-sea convection in the northwestern Mediterranean during winter 2012, *Geophys. Res. Lett.*, *40*, 1379–1385, doi:10.1002/grl.50331.
Estournel, C., V. Zervakis, P. Marsaleix, A. Papadopoulos, F. Auclair, L. Perivoliotis, and E. Tragou (2005), Dense water formation and cascading in the Gulf of Thermaikos (North Aegean) from observations and modelling, *Cont. Shelf Res.*, *25*, 2366–2386, doi:10.1016/j.csr.2005.08.014.
Estournel, C., F. Auclair, M. Lux, C. Nguyen, and P. Marsaleix (2009), "Scale oriented" embedded modeling of the North-Western Mediterranean in the frame of MFSTEP, *Ocean Sci.*, *5*, 73–90.
Fasham, M. J. R., K. J. Flynn, P. Pondaven, T. R. Anderson, and P. W. Boyd (2006), Development of a robust marine ecosystem model to predict the role of iron in biogeochemical cycles: A comparison of results for iron-replete and iron-limited areas, and the SOIREE iron-enrichment experiment, *Deep Sea Res., Part 1*, *53*, 333–366.
Font, J., P. Puig, J. Salat, A. Palanques, and M. Emelianov (2007), Sequence of hydrographic changes in the NW Mediterranean deep water due to exceptional winter 2005, *Sci. Mar.*, *72*, 339–346.
Gaspar, P., Y. Grégoris, and J. M. Lefevre (1990), A simple kinetic energy model for simulations of the oceanic vertical mixing: Testsat station papa and long-term upper ocean study site, *J. Geophys. Res.*, *95*, 16,179–16,193.
Geider, R. J., H. L. Macintyre, L. M. Graziano, and R. M. L. McKay (1998), Responses of the photosynthetic apparatus of Dunaliella tertiolecta (Chlorophyceae) to nitrogen and phosphorus limitation, *Eur. J. Phycol.*, *33*, 315–332.
Gernez, P. (2009), Analyse de la variabilité temporelle des propriétés optiques en mer Ligure depuis un mouillage instrumenté (site Boussole): Fluctuations à haute fréquence, cyclicité diurne, changements saisonniers et variabilité interannuelle Temporal variability of the biooptical properties in the North-Western Mediterranean sea (BOUSSOLE site), PhD thesis, Univ. Pierre et Marie Curie, France.
Gogou, A., et al. (2014), Reprint of: Carbon flux to the deep in three open sites of the Southern European Seas (SES), *J. Mar. Syst.*, *135*, 170–179, doi:10.1016/j.jmarsys.2014.04.012.
Goldman, J. G., D. A. Caron, and M. R. Dennett (1987), Nutrient cycling in a microflagellate food chain: IV. Phytoplankton microflagellate interactions, *Mar. Ecol. Prog. Ser.*, *38*, 75–87.
Gorbunov, M. Y., Z. S. Kolber, and P. G. Falkowski (1999), Measuring photosynthetic parameters in individual algal cells by Fast Repetition Rate fluorometry, *Photosynth. Res.*, *62*, 141–153.
Hansen, P. J., P. K. Bjørnsen, and B. W. Hansen (1997), Zooplankton grazing and growth: Scaling within the 2–2,000-μm body size range, *Limnol. Oceanogr.*, *42*, 687–704.
Harrison, W. G., L. R. Harris, and B. D. Irwin (1996), The kinetics of nitrogen utilization in the oceanic mixed layer: Nitrate and ammonium interactions at nanomolar concentrations, *Limnol. Oceanogr.*, *41*, 16–32.
Heimbürger, L. E., H. Lavigne, C. Migon, F. D'Ortenzio, C. Estournel, L. Coppola, and J.-C. Miquel (2013), Temporal variability of vertical export flux at the DYFAMED time-series station (Northwestern Mediterranean Sea). *Prog. Oceanogr.*, *119*, 59–67.
Herrmann, M. (2007), Formation et devenir des masses d'eau en Méditerranée Nord-Occidentale, Influence sur l'écosysteme plantonique pélagique, Variabilité interannuelle et changement climatique, PhD thesis, Univ. Toulouse III Paul Sabatier, Toulouse, France.
Herrmann, M., and S. Somot (2008), Relevance of ERA40 dynamical downscaling for modeling deep convection in the Mediterranean Sea, *Geophys. Res. Lett.*, *35*, L04607, doi:10.1029/2007GL032442.
Herrmann, M., S. Somot, F. Sevault, C. Estournel, and M. Déqué (2008), Modeling the deep convection in the Northwestern Mediterranean sea using an eddy-permitting and an eddy-resolving model: Case study of winter 1986–87, *J. Geophys. Res.*, *113*, C04011, doi:10.1029/2006JC003991.
Herrmann, M., F. Sevault, J. Beuvier, and S. Somot (2010), What induced the exceptional 2005 convection event in the northwestern Mediterranean basin? Answers from a modeling study, *J. Geophys. Res.*, *115*, C08029, doi:10.1029/2009JC005749.
Herrmann, M., F. Diaz, C. Estournel, P. Marsaleix, and C. Ulses (2013), Impact of atmospheric and oceanic interannual variability on the Northwestern Mediterranean Sea pelagic planktonic ecosystem and associated carbon cycle, *J. Geophys. Res. Oceans*, *118*, 5792–5813, doi:10.1002/jgrc.20405.
Herrmann M, C. Estournel, F. Adloff, and F. Diaz (2014), Impact of Climate change on the Northwestern Mediterranean Sea pelagic planktonic ecosystem and associated carbon cycle, *J. Geophys. Res. Oceans*, *119*, 5815–5836, doi:10.1002/2014JC010016.
Houpert, L. (2013), Contribution to the study of transfer processes from the surface to the deep ocean in the Mediterranean sea using in-situ measurements, PhD thesis, Univ. of Perpignan, France.
Lacroix, G., and M. Grégoire (2002), Revisited ecosystem model (MODECOGeL) of the Ligurian Sea: Seasonal and interannual variability due to atmospheric forcing, *J. Mar. Syst.*, *37*, 229–258.
Laney, S. R., R. M. Letelier, and M. R. Abbott (2005), Parameterizing the natural fluorescence kinetics of Thalassiosira weissflogii, *Limnol. Oceanogr.*, *50*, 1499–1510.
Lavigne, H. (2013), Impact of mixed layer depth seasonal variations on the phytoplankton phenology in the Mediterranean Sea, PhD thesis, Univ. Pierre et Marie Curie, Paris, France.
Lavigne, H., F. D'Ortenzio, C. Migon, H. Claustre, P. Testor, M. R. d'Alcalà, R. Lavezza, L. Houpert, and L. Prieur (2013), Enhancing the comprehension of mixed layer depth control on 1157 the Mediterranean phytoplankton phenology, *J. Geophys. Res. Oceans*, *118*, 3416–3430, doi:10.1002/jgrc.20251.

Liu, H., and M. Dagg (2003), Interactions between nutrients, phytoplankton growth, and micro- and mesozooplankton grazing in the plume of the Mississippi River, *Mar. Ecol. Prog. Ser.*, *258*, 31–42.
Lopez-Jurado, J.-L., C. Gonzalez-Pola, and P. Velez-Belchı (2005), Observation of an abrupt disruption of the long-term warming trend at the Balearic Sea, western Mediterranean Sea, in summer 2005, *Geophys. Res. Lett.*, *32*, L24606, doi:10.1029/2005GL024430.
Marsaleix, P., F Auclair, and C. Estournel (2006), Considerations on open boundary conditions for regional and coastal ocean models, *J. Atmos. Oceanic Technol.*, *23*, 1604–1613, doi:10.1175/JTECH1930.1.
Marsaleix, P., F. Auclair, J. W. Floor, M. J. Herrmann, C. Estournel, I. Pairaud, and C. Ulses (2008), Energy conservation issues in sigma-coordinate free-surface ocean models, *Ocean Modell.*, *20*, 61–89, doi:10.1016/j.ocemod.2007.07.005.
Marsaleix, P., F. Auclair, and C. Estournel (2009), Low-order pressure gradient schemes in sigma coordinate models: The seamount test revisited, *Ocean Modell.*, *30*, 169–177, doi:10.1016/j.ocemod.2009.06.011.
Marsaleix, P., F. Auclair, C. Estournel, C. Nguyen, and C. Ulses (2011), An accurate implementation of the compressibility terms in the equation of state in a low order pressure gradient scheme for sigma coordinate ocean models, *Ocean Modell.*, *40*, 1–13, doi:10.1016/j.ocemod.2011.07.004.
Marsaleix, P., F. Auclair, T. Duhaut, C. Estournel, C. Nguyen, and C. Ulses (2012), Alternatives to the Robert-Asselin filter, *Ocean Modell.*, *41*, 53–66.
Martín, J., and J.-C. Miquel (2010), High downward flux of mucilaginous aggregates in the Ligurian Sea during summer 2002: Similarities with the mucilage phenomenon in the Adriatic Sea, *Mar. Ecol.*, *31*, 393–406.
Martin, J. H., G. Knauer, D. M. Karl, and W. W. Broenkow (1987), VERTEX: Carbon cycling in the northeast Pacific, *Deep Sea Res., Part A*, *34*(2), 267–285.
Martin, J., J.-C. Miquel, and A. Khripounoff (2010), Impact of open sea deep convection on sediment remobilization in the western Mediterranean, *Geophys. Res. Lett.*, *37*, L13604, doi:10.1029/2010GL043704.
Marty, J.-C., and J. Chiavérini (2002), Seasonal and interannual variations in phytoplankton production at DYFAMED time-series station, northwestern Mediterranean Sea, *Deep Sea Res., Part 2*, *49*, 2017–2030.
Marty, J.-C., and J. Chiavérini (2010), Hydrological changes in the Ligurian Sea (NW Mediterranean, DYFAMED site) during 1995–2007 and biogeochemical consequences, *Biogeosciences*, *7*, 2117–2128.
Marty, J.-C., J. Chiavérini, M. D. Pizay, and B. Avril (2002), Seasonal and interannual dynamics of nutrients and phytoplankton pigments in the western Mediterranean Sea at the DYFAMED time-series station (1991–1999), *Deep Sea Res. Part II*, *49*, 1965–1985.
MEDOC Group (1970), Observation of formation of deep water in the Mediterranean Sea, *Nature*, *227*(1037), 1040.
Mertens, C., and F. Schott (1998), Interannual variability of deep-water formation in the northwestern Mediterranean, *J. Phys. Oceanogr.*, *28*, 1410–1424.
Migon, C., V. Sandroni, J.-C. Marty, B. Gasser, and J.-C. Miquel (2002), Transfer of atmospheric matter through the euphotic layer in the northwestern Mediterranean: Seasonal pattern and driving forces, *Deep Sea Res., Part II*, *49*, 2125–2141.
Miquel, J. C., S. W. Fowler, J. La Rosa, and P. Buat-Ménard (1994), Dynamics of the downward flux of particles and carbon in the open northwestern Mediterranean Sea, *Deep Sea Res., Part I*, *41*, 243–261.
Miquel J.-C., J. Martín, B. Gasser, A. Rodriguez-y-Baena, T. Toubal, and S.W. Fowler (2011), Dynamics of particle flux and carbon export in the northwestern Mediterranean Sea: A two decade time-series study at the DYFAMED site, *Prog. Oceanogr.*, *91*, 461–481.
Moore, C. M., D. Suggett, P. M. Holligan, J. Sharples, E. R. Abraham, M. I. Lucas, T. P. Rippeth, N. R. Fisher, J. H. Simpson, and D. J. Hydes (2003), Physical controls on phytoplankton physiology and production at a shelf sea front: A fast repetition-rate fluorometer-based field study, *Mar. Ecol. Prog. Ser.*, *259*, 29–45.
Moutin, T., P. Raimbault, H. Golterman, and B. Coste (1998), The input of nutrients by the Rhône river into the Mediterranean Sea: Recent observations and comparison with earlier data, *Hydrobiologia*, *373–374*, 237–246.
Nash, J. E., and J. V. Sutcliffe (1970), River flow forecasting through conceptual models part I: A discussion of principles, *J. Hydrol.*, *10*(3), 282–290.
Nejstgaard, J. C., I. Gismervik, and P. T. Solberg (1997), Feeding and reproduction by Calanus finmarchicus, and microzooplankton grazing during mesocosm blooms of diatoms and the coccolithophore Emiliania huxleyi, *Mar. Ecol. Prog. Ser.*, *147*, 197–217.
Oliver, R. L., J. Whittington, Z. Lorenz, and I. T. Webster (2003), The influence of vertical mixing on the photoinhibition of variable chlorophyll a fluorescence and its inclusion in a model of phytoplankton photosynthesis, *J. Plankton Res.*, *25*, 1107–1129.
Pasqueron de Fommervault, O., C. Migon, F. D'Ortenzio, M. Ribera d'Alcalà, and L. Coppola (2015), Temporal variability of nutrient concentrations in the northwestern Mediterranean sea (DYFAMED time-series station), *Deep Sea Res., Part I*, *100*, 1–12.
Pastor, L., C. Cathalot, B. Deflandre, E. Viollier, K. Soetaert, F. J. R. Meysman, C. Ulses, E. Metzger, and C. Rabouille (2011), Modeling biogeochemical processes in sediments from the Rhone River prodelta area (NW Mediterranean Sea), *Biogeosciences*, *8*, 1351–1366.
Prieur, L., and L. Legendre (1988), Oceanographic criteria for new phytoplankton production. NATO ASI Series. Series C, *Math. Phys. Sci.*, *239*, 71–112.
Pujo-Pay, M., and P. Conan (2003), Seasonal variability and export of dissolved organic nitrogen in the Northwestern Mediterranean Sea, *J. Geophys. Res.*, *108*(C6), 3188, doi:10.1029/2000JC000368.
Raick, C., E. J. M. Delhez, K. Soetaert, and M. Grégoire (2005), Study of the seasonal cycle of the biogeochemical processes in the Ligurian Sea using a 1D interdisciplinary model, *J. Mar. Syst.*, *55*, 177–203.
Reffray, G., P. Fraunié, and P. Marsaleix (2004), Secondary flows induced by wind forcing in the Rhône region of freshwater influence, *Ocean Dyn.*, *54*, 179–196.
Riegman, R., W. Stolte, A. A. M. Noordeloos, and D. Slezak (2000), Nutrient uptake and alkaline phosphatase (ec 3:1:3:1) activity of emiliania huxleyi (Prymnesiophyceae) during growth under n and p limitation in continuous cultures, *J. Phycol.*, *36*, 87–96.
Santinelli, C., L. Nannicini, and A. Seritti (2010), DOC dynamics in the meso and bathypelagic layers of the Mediterranean Sea, *Deep Sea Res., Part II*, *57*, 1446–1459.
Sarthou, G., K. R. Timmermans, S. Blain, and P. Tréguer (2005) Growth physiology and fate of diatoms in the ocean: A review, *J. Sea. Res.*, *53*, 25–42.
Schroeder, K., A. Ribotti, M. Borghini, R. Sorgente, A. Perilli, and G. P. Gasparini (2008), An extensive western Mediterranean deep water renewal between 2004 and 2006, *Geophys. Res. Lett.*, *35*, L18605, doi:10.1029/2008GL035146.
Sempéré, R., B. Charrière, F. Van Wambeke, and G. Cauwet (2000), Carbon Inputs of the Rhône River to the Mediterranean Sea: Biogeochemical Implications, *Global Biogeochem. Cycles*, *14*, 669–681.
Severin, T., P. Conan, X. Durrieu de Madron, L. Houpert, M. J. Oliver, L. Oriola, J. Caparros, J. F. Ghiglione, and M. Pujo-Pay (2014), Impact of open-ocean convection on nutrients, phytoplankton biomass and activity, *Deep Sea Res. Part I*, *94*, 62–71. doi:10.1016/j.dsr.2014.07.015.
Siegel, D., S. Doney, and J. Yoder (2002), The North Atlantic spring phytoplankton bloom and Sverdrup's critical depth hypothesis, *Science*, *296*, 730–733.

Smith, R. O., H. L. Bryden, and K. Stansfield (2008), Observations of new western Mediterranean deep water formation using Argo floats 2004–2006, *Ocean Sci.*, *4*, 133–149.
Soetaert, K., J. J. Middelburg, P. M. J. Herman, and K. Buis (2000), On the coupling of benthic and pelagic biogeochemical models, *Earth Sci. Rev.*, *51*, 173–201.
Soetaert, K., P. M. J. Herman, J. J. Middelburg, C. Heip, C. L. Smith, P. Tett, and K. Wild-Allen (2001), Numerical modelling of the shelf break ecosystem: Reproducing benthic and pelagic measurements, *Deep Sea Res., Part II*, *48*, 3141–3177.
Soetaert, K., A. F. Hofmann, J. J. Middelburg, F. Meysman, and J. Greenwood (2007), The effect of biogeochemical processes on pH, *Mar. Chem.*, *105*, 30–51.
Sondergaard, M., and J. Theil-Nielsen (1997), Bacterial growth efficiency in lakewater cultures, *Aquat. Microb. Ecol.*, *12*, 115–122.
Somot, S., F. Sevault, and M. Déqué, (2006), Transient climate change scenario simulation of the Mediterranean Sea for the 21st century using a high resolution ocean circulation model, *Clim. Dyn.*, *27*, 1–29, doi:10.1007/s00382-006-0167-z.
Stabholz M., X. Durrieu de Madron, A. Khripounoff, M. Canals, I. Taupier-Letage, P. Testor, S. Heussner, P. Kerhervé, L. Houpert, and N. Delsaut (2013), Impact of open-sea convection on particulate fluxes and sediment dynamics in the deep basin of the Gulf of Lions, *Biogeosciences*, *10*, 1097–1116.
Tanaka, T., and F. Rassoulzadegan (2002), Full-depth profile (0–2000 m) of bacteria, heterotrophic nanoflagellates and ciliates in the NW Mediterranean Sea: Vertical partitioning of microbial trophic structures, *Deep Sea Res., Part II*, *49*, 2093–2107.
Taylor, K. E. (2001), Summarizing multiple aspects of model performance in a single diagram, *J. Geophys. Res.*, *106*, 7183–7192.
Timmermans, K. R., B. Van der Wagt, M. J. W. Veldhuis, A. Maatman, and H. J. W. De Baar (2005), Physiological responses of three species of marine pico-phytoplankton to ammonium, phosphate, iron and light limitation, *J. Sea Res.*, *53*, 109–120.
Thingstad, T. F. (2005), Simulating the response to phosphate additions in the oligotrophic eastern Mediterranean using an idealized four-member microbial food web model, *Deep Sea Res., Part. II*, *52*, 3074–3089.
Thingstad, T. F., E. F. Skjoldal, and R. A. Bohne (1993), Phosphorus cycling and algal-bacterial competition in Sandsfjord, western Norway, *Mar. Ecol. Prog. Ser.*, *99*, 239–259.
Tyrrell, T., and A. H. Taylor (1996), A modelling study of Emiliania huxleyi in the NE Atlantic, *J. Mar. Syst.*, *9*, 83–112.
Uitz, J., H. Claustre, A. Morel, and S. B. Hooker (2006), Vertical distribution of phytoplankton communities in open ocean: An assessment based on surface chlorophyll, *J. Geophys. Res.*, *111*, C08005, doi:10.1029/2005JC003207.
Uitz, J., D. Stramski, B. Gentili, F. D'Ortenzio, and H. Claustre (2012), Estimates of phytoplankton class-specific and total primary production in the Mediterranean Sea from satellite ocean color observations, *Global Biogeochem. Cycles*, *26*, GB2024, doi:10.1029/2011GB004055.
Ulses, C., C. Estournel, P. Puig, X. Durrieu de Madron, and P. Marsaleix (2008), Dense shelf water cascading in the northwestern Mediterranean during the cold winter 2005: Quantification of the export through the Gulf of Lion and the Catalan margin, *Geophys. Res. Lett.*, *35*, L07610, doi:10.1029/2008GL033257.
Van den Meersche, K., J. J. Middelburg, K. Soetaert, P. van Rijswijk, H. T. S. Boschker, and C. H. R. Heip (2004), Carbon-nitrogen coupling and algal-bacterial interactions during an experimental bloom: Modeling a ^{13}C tracer experiment, *Limnol. Oceanogr.*, *49*(3), 862–878, doi: 10.4319/lo.2004.49.3.0862.
Vichi, M., N. Pinardi, and S. Masina (2007), A generalized model of pelagic biogeochemistry for the global ocean ecosystem. Part I: Theory, *J. Mar. Syst.*, *64*, 89–109.
Walin, G. (1982), On the relation between sea-surface heat flow and the thermal circulation in the ocean, *Tellus*, *34*, 187–195.

Erratum

In the originally published version of this article, the first two rows of Table 2 were omitted. The footnote for Table 2 was also published incorrectly. These instances have since been corrected, and this version may be considered the authoritative version of record.